EFFECTS OF OXYGEN-18 SUBSTITUTION UPON ELECTRONIC RELAXATION IN SO_2

A THESIS

Presented to

The Faculty of the Graduate Division

by

Glenn Edward Nelson

In Partial Fulfillment

of the Requirements for the Degree

Master of Science in Chemistry

Georgia Institute of Technology

August 1973

EFFECTS OF OXYGEN-18 SUBSTITUTION

UPON ELECTRONIC RELAXATION IN SO_2

Approved:

Chairman

Date Approved by Chairman: Aug. 15, 1973

ACKNOWLEDGEMENTS

First and foremost I want to thank our Lord in Heaven for giving me the ability and perseverance to complete this research effort and I pray that this thesis will serve to glorify His name.

Dr. Raymond Borkman, my research advisor, deserves my thanks for suggesting this problem and for providing day-to-day counsel on its solution. Feeling not that I was working "for" him, but instead that I was working "with" him was a most rewarding experience. He has a knack for straddling the academic fence that so often separates the good scientists from the good human beings and consequently he was both a mentor and a friend. I will not soon forget him or the influence he has had upon me.

I would like to thank my parents for having confidence in, and encouragement for, me throughout my academic endeavors, and do sincerely appreciate their continued support of my morale.

Finally, I want to thank Dr. Harry Hopkins of the Department of Chemistry of Georgia State University for unknowingly providing our group with a phrase that has echoed in our laboratory many, many times. As he said, "You've got to be good to do low temperature work." And we were.

TABLE OF CONTENTS

LIST OF TABLES

LIST OF TABLES (Continued)

LIST OF ILLUSTRATIONS

CHAPTER I

INTRODUCTION AND BACKGROUND

When a polyatomic molecule A absorbs light in the visible or near ultraviolet region, an electronically excited molecule A** is produced. The excited species may return to its initial unexcited state by any of several processes or by some combination of them. The processes are:

1. Direct or indirect radiationless relaxation in which none of the absorbed light is re-emitted. In this case, the electronic excitation energy is first converted into vibrational or rotational energy which is then transferred to the environment in the form of heat.

2. Emission of light which is not normally of the same wavelength as the exciting light. This emission may be directly from the initially prepared excited state or from some subsequent excited electronic state(s) A* which are lower in energy than the initial state and which have been populated through radiationless transitions.

3. Photochemical reaction which results in the production of a new chemical species. Such a process may originate with the initially prepared excited state or from some subsequent lower energy excited state which has been populated by radiationless transitions from the higher energy initial state.

4. Electronic energy transfer where either A** or A* transfers electronic energy to another molecule B (which is generally different from A) to produce an electronically excited state B*.

The research presented herein dealt exclusively with the first two relaxation pathways. The terminology associated with radiative and radiationless transitions is presented in Figure 1. The first excited singlet state of some molecule is shown to be of higher energy than the first excited triplet state, and both of them are of higher energy than the ground singlet state. Absorption of light of appropriate wavelength can cause an electronic transition to take place and create either the first excited singlet state or the first excited triplet state. The resultant state depends, of course, upon the wavelength of the absorbed excitation light. If the first singlet is the prepared state it may relax electronically to the ground state via either of two pathways. The process which is most direct and which involves emission of light is termed "fluorescence." The alternate path first involves a radiationless transition to the first triplet state and is termed "intersystem crossing." At that point there are yet two more relaxation pathways open to the molecule. Radiative relaxation to the ground state is termed "phosphorescence" and is typically a much longer process (e.g. 10^4) than fluorescence since it is a spin-forbidden process by the selection rules of quantum mechanics. The final possibility is for the triplet state to decay radiationlessly to the ground state.

It was first discovered in 1960 (1) and 1961 (2) that substitution of deuterium in aromatic hydrocarbon molecules could have a dramatically large effect upon the lifetime of the first excited triplet state. Hutchison and Mangum (1) noted that the phosphorescence lifetime of deuterated naphthalene in a solvent of deuterated durene at $77^{\circ}K$ increased from 2.1 ± 0.1 seconds to 16.9 ± 0.7 seconds upon

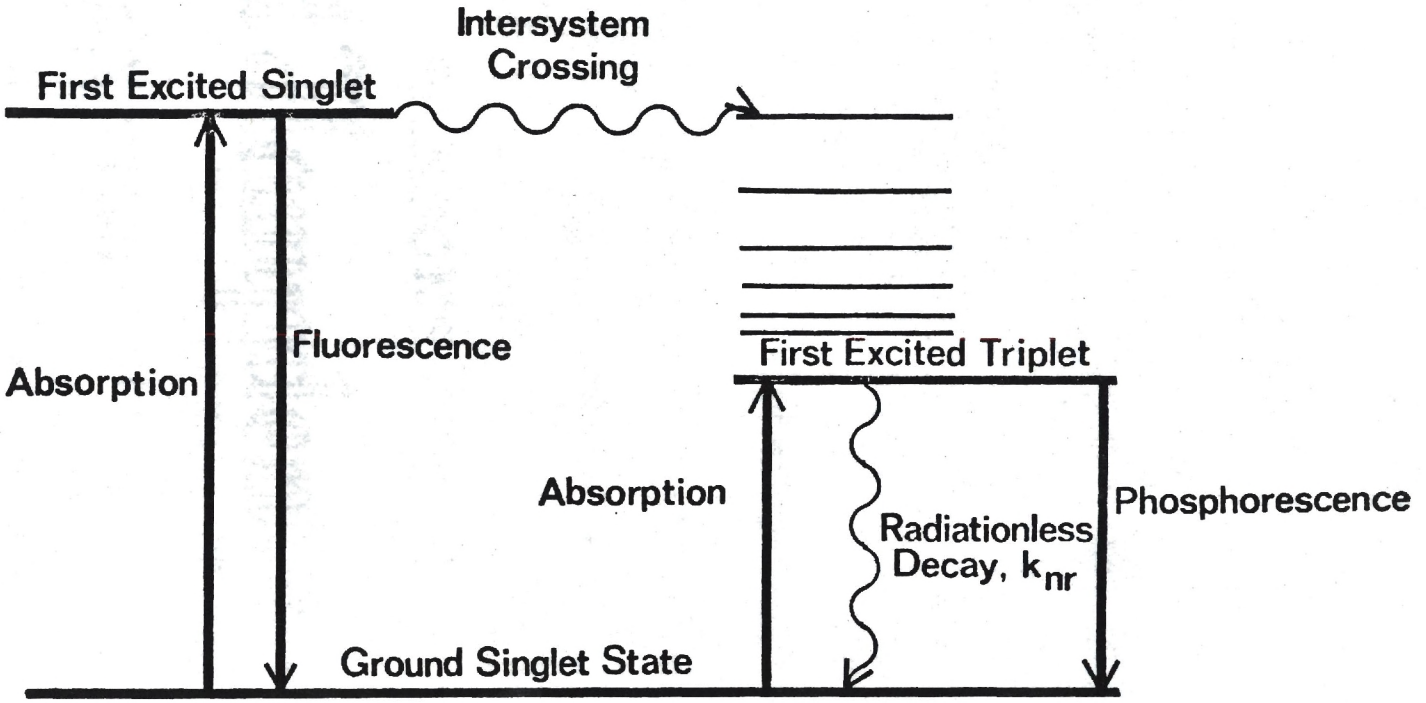

Fig. 1. Terminology of Triplet Relaxation.

deuteration. They postulated that this 800 percent effect was due to the mass effect upon singlet-triplet interconversion rates and upon the rate of electronic energy transfer to the host crystal.

Since that time it has been shown that perdeuteration produces a similar effect in both ketones (5-8) and aldehydes (9,10). Borkman and Kearns (5) found that the phosphorescence lifetime of acetone-d_6 in rigid ether-IPA glass at 77°K was 250 percent longer than the undeuterated species and concluded that the mechanism of electronic relaxation involved to some extent the C-H stretching vibrations. Lamola (6) studied acetophenone and acetophenone-d_5 in three solvents at 77°K and observed a 9-49 percent increase in the phosphorescence lifetime. He suggested two second order mechanisms which could give some allowed character to the otherwise spin-forbidden transition. The first was for the triplet state to be vibronically coupled to the $^3n, \pi^*$ state and for this latter state to be spin-orbit coupled to the singlet state. The second mechanism involved spin-orbit coupling between the triplet and the $^1n, \pi^*$ state with vibronic coupling of the latter state to the singlet state.

Partially deuterated species have also been studied (4,6,9-15). Martin and Kalantar (4) in 1968 measured the phosphorescence decay times of perdeuterated benzene and two partially deuterated benzenes in 3 solvents at 77°K. They found that the lifetime ratios for C_6H_6, C_6H_5D, C_6HD_5, and C_6D_6 were 1:1.06:1.5:2.0, respectively. Lin and Bersohn (14) in 1968 studied partially deuterated naphthalenes and discovered that the decay rate varied linearly with the number of deuterons in the molecule but there was no dependence of the decay rate upon which positions were substituted.

It was not until 1968 that any isotope effect other than a deuterium effect was studied. At that time Martin and Kalantar (4) substituted carbon-13 in benzene and measured the phosphorescence lifetimes in three solvents at 77°K. There was no measurable increase in the lifetime and this led to the conclusion that the point group symmetry of the benzene isomer was not an important factor in determining the nonradiative rate constant. Borkman and Yamanashi (16) in 1972 studied acetone and acetone-^{18}O in both EPA glass and neat crystals at 77°K and found that the substituted species exhibited a 10 percent lifetime increase over that of normal acetone.

The research efforts presented above have documented the existence of a pronounced isotope effect upon the phosphorescence lifetimes of many organic molecules. However, due to the complexity of these molecules an exact assignment of the precise mechanism of the isotope effect has proven vexing. In the research effort presented herein, it was hoped that selection of a relatively simple molecule, sulfur dioxide, for further isotope studies would permit a thorough elucidation of the mechanism of the effect. Specifically, the phosphorescence lifetimes of sulfur dioxide and of oxygen-18 substituted sulfur dioxide have been determined in the solid state at 77°K, 4.2°K, and 1.4°K. Combining these with measurements of the quantum yield for phosphorescence, it has been possible to calculate the magnitude of the isotope effect upon the radiative and nonradiative rate constants for the decay of the triplet state.

It should be pointed out that selection of SO_2 for this study was not done at random. Other likely candidates for such a study

might seem to be molecules such as NO_2, CO_2, or O_3. However neither NO_2 nor O_3 phosphoresce although they do absorb in the visible region (17). CO_2 absorbs in neither the visible nor the near-UV and does not phosphoresce (17). On the other hand SO_2 does phosphoresce with moderate strength as a solid and its absorption and emission spectra have been carefully analyzed (18-22,37,39). Since this research effort hoped to characterize the mechanism by which the forbidden triplet-singlet transition acquired some allowed character, having analyses available for the emission and absorption spectra was an important consideration indeed.

Although there have been several previous studies on the phosphorescence emission properties of SO_2 (23,24), the nature of the nonradiative processes which compete effectively with the radiative processes has not been characterized. Fluorescence quantum yields for SO_2 vapor have been reported (25,26) but no value has been obtained previous to this work for phosphorescence quantum yields at $77^{o}K$ and $4.2^{o}K$. Finally, no work previous to this has studied the temperature dependence of the radiative and nonradiative rate constants for either SO_2 or oxygen-18 substituted SO_2.

CHAPTER II

APPARATUS AND EXPERIMENTAL DETAIL

The experimental effort was dedicated to determining precisely what portion of the SO_2 excited triplet states returned to the ground state via each of the available electronic relaxation pathways and to determining the rates of these decay processes. The materials, equipment, and procedures used in making these measurements are discussed in the following order:

1. materials,
2. spectra,
3. phosphorescence quantum yields, and
4. phosphorescence lifetimes.

Materials and Sample Preparation

The $S^{16}O_2$ (Matheson, anhydrous grade) was analyzed to be 99.9 mole percent pure and was used without further purification. The $S^{18}O_2$ (Miles-Yeda Laboratories) was stated by the manufacturer to be of 92.6 mole percent isotopic purity and was used as supplied. At the end of all experimentation, mass spectral analysis showed the sample to be of 70 mole percent isotopic purity. The samples were contained in sealed glass sample cells having lower sections made from 3 mm I.D. quartz tubing. All gas transfers were made in the high-vacuum manifold through breakseal connections which were broken with an iron rod encased with glass. All samples were degassed through three freeze-pump-thaw cycles

to 3 x 10^{-5} Torr and were sealed off while frozen at 77°K and while the cell was being evacuated.

It was found that stronger phosphorescence occurred when the SO_2 sample was solidified slowly rather than abruptly solidified. The sample was first liquefied in a dry ice and ethanol bath and then liquid nitrogen was slowly added in several small portions with vigorous stirring until the bath temperature was lowered to around 165°K. At that time the sample was transferred to a liquid nitrogen bath and maintained there for the duration of the experiment or until lowered into liquid helium.

Spectra

Absorption Spectra

Gas phase absorption spectra were measured in a round cell (2.25 cm I.D.) with a 9.75 cm path length and having quartz windows. A Cary-14 absorption spectrometer was used for studying the singlet-singlet regions and a Beckman Octa-5 with a 0.0 - 0.1 optical density full scale sensitivity was used for studying the very weak singlet-triplet absorption. To eliminate the possibility that Beer's law might not apply to very dilute gases (27), a calibration curve was generated to make sure that optical density did indeed vary linearly with concentration in the regions under study.

Phosphorescence Emission Spectra

All phosphorescence emission spectra were obtained with the following apparatus (see Figure 2):

1. an optical excitation system composed of a suitable light source and a monochromator with interference filter;

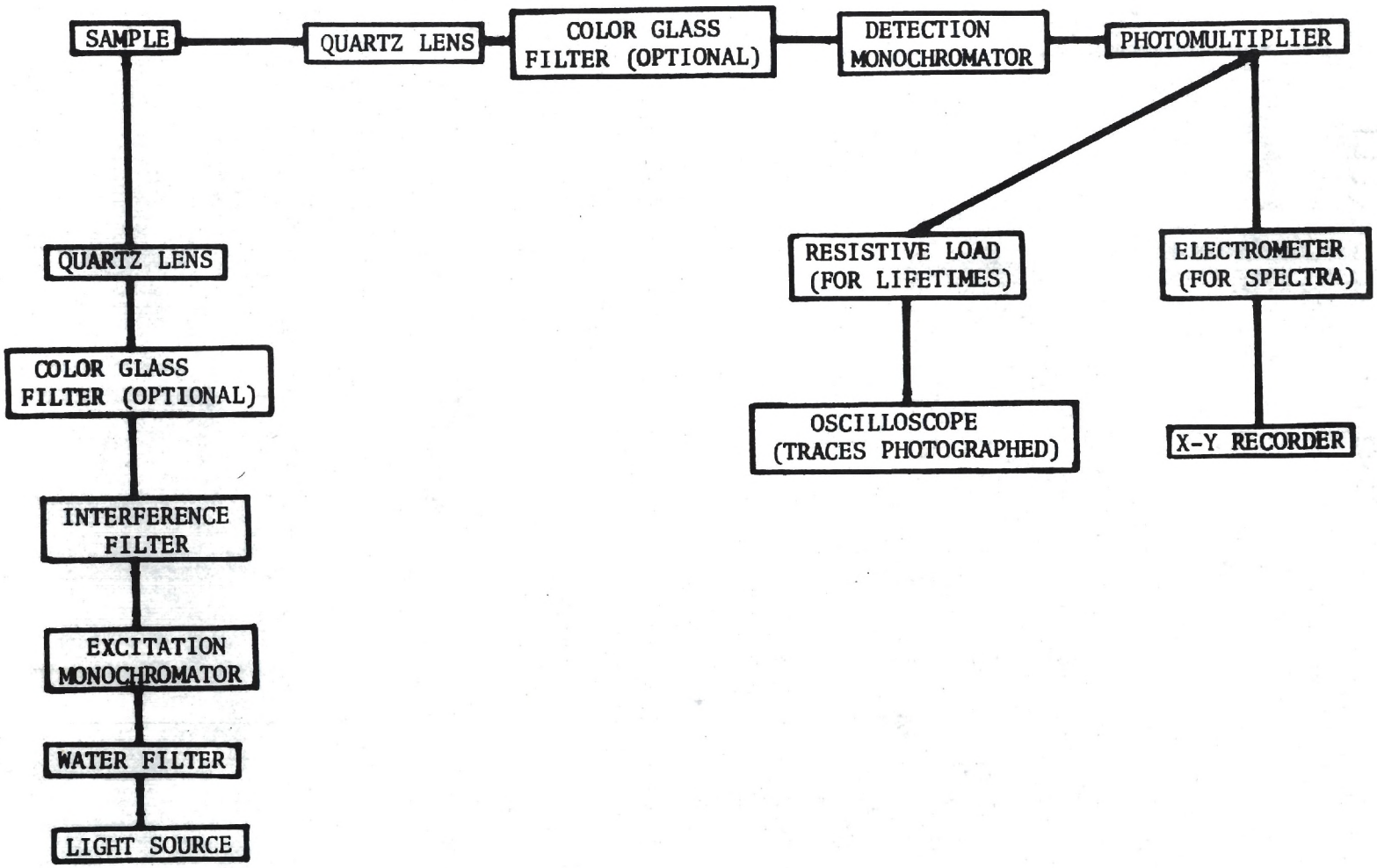

Fig. 2. Schematic of Experimental Apparatus.

2. a sample compartment containing a vernier - geared sample holder for optimization, a dewar, and a rotating mechanical chopper;

3. an emission detection system composed of a monochromator, phototube, and amplifier.

Optical Excitation System. Three continuous light sources were used for obtaining spectra. They were a 1000 watt xenon lamp (Oriel Optics Corp. model C-46-61-5), a 500 watt mercury lamp (Oriel model C-46-61-4) and a 100 watt high-pressure mercury point source lamp (P.E.K. Labs model 401). The latter source was the most frequently used since the arc was quite small and with proper focusing most of its energy could be contained within a one millimeter beam.

The output of the light source passed through a water filter to remove infra-red radiation and into a high intensity UV/visible grating monochromator (Bausch and Lomb model 33-86-26-07) with a dispersion of 74 Angstroms per millimeter and blazed for 2100 Angstroms. The entrance slit width/exit slit width ratio was maintained at 1.7/1.0 as recommended by the manufacturer to give maximum spectral purity and was calibrated relative to a low pressure mercury light source. The monochromator was fitted with a synchronous motor (Cramer model 1401, 1 rph) which permitted the wavelength to be varied at a fixed rate of 2 Angstroms per second if desired. The output of the monochromator passed through a 3650 Angstrom interference filter (Ealing-TFP) and into a quartz lens which focused the exciting light onto the sample in the sample compartment.

Sample Compartment. The sample compartment is a completely enclosed aluminum box with its interior painted a flat black color to

minimize reflections. It lies at the perpendicular intersection of two optical benches such that excitation of the sample takes place along one of the benches and detection takes place along the other. The sample is held in the optical path by a spring-loaded sample holder mounted on a two-axis vernier drive such that the position of the sample can be optimized with respect to both the excitation beam and the detection path. The sample was placed in a partially-silvered quartz dewar for 77°K studies and in a specially constructed helium dewar (Figure 3) for studies at 4.2°K and 1.4°K. The helium dewar was constructed by Mr. Don Lilley and Mr. Jim Kinloch of the Chemistry Department's glass lab and the dolly for transporting and positioning the dewar was constructed by Mr. Malcolm Rucker, machinist for the Chemistry Department. A rotating double-slit mechanical chopper was installed around the dewar and in the optical path to prevent fluorescence and scattered light from reaching the photomultiplier. Since it was desirable to run the chopper no faster than actually needed, a Variac was used as a speed control.

The liquid helium dewar was placed in the sample compartment for studies at 4.2°K and 1.4°K. Supercooling of the liquid helium to 1.4°K was accomplished by pumping the helium in the inner dewar. The two pumps used for this purpose were a low capacity Welch Duo-Seal model 1405 (60 lpm) with a diffusion pump and a nitrogen cold trap, and a high capacity Welch Duo-Seal model 1397B (500 lpm). A U-tube manometer filled with n-butyl phthalate was used to determine the vapor pressure of the supercooled liquid helium and subsequently the temperature (28).

The process by which the helium dewar was prepared for usage was a rather involved one that began with evacuating the jacket of the inner

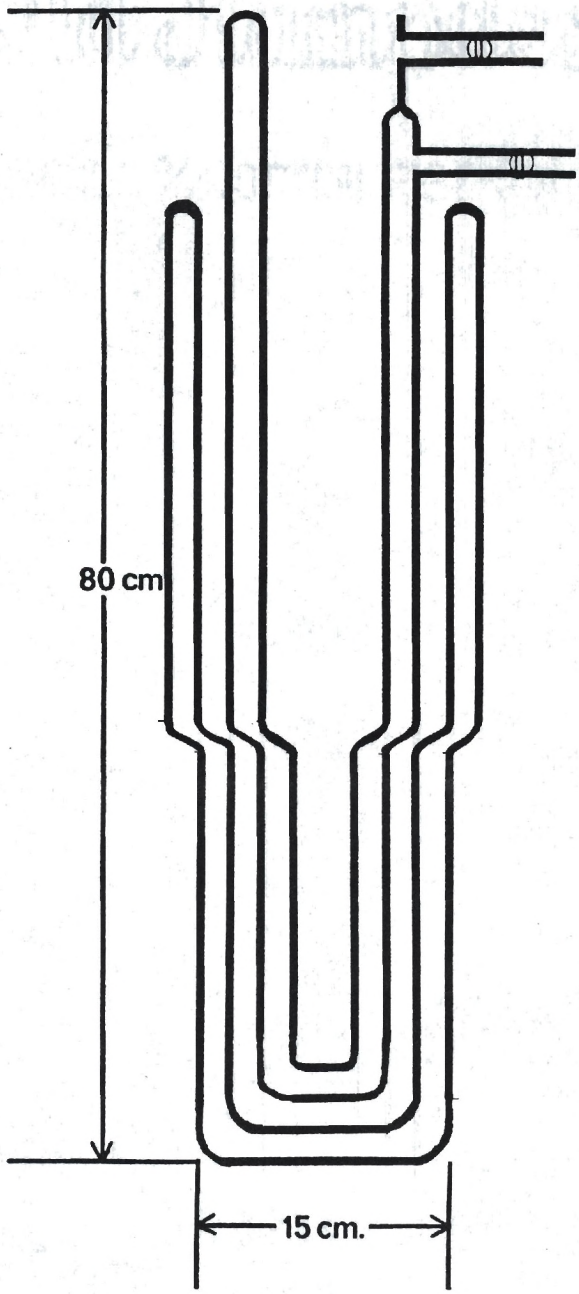

Fig. 3. Helium Dewar.

dewar to a pressure of 5×10^{-6} Torr in order to remove any helium from the jacket that might have diffused through the walls during the previous experiment. Concurrently, any moisture present in the inner dewar was removed and a nitrogen purging tube was pushed to the bottom of the inner dewar. The dewar lid was then positioned in place such that when the dry nitrogen gas purge began there would only be one small exit for the gas at the top of the dewar and all moisture-laden air could be effectively removed. The inner dewar was purged for at least 20 minutes and then the outer dewar was filled with liquid nitrogen. After one and one half hours of nitrogen purging the inner dewar was quite cold and the purging line was rapidly disconnected from the nitrogen source and reconnected to a dry helium gas source. The helium purge lasted for at least 30 minutes and the purge was stopped only at the very last moment before the transfer of the liquid helium was to begin.

At that time the low pressure release valve on the helium tank was plugged and the helium purging line was connected to the liquid helium transfer tube and purged vigorously with dry helium gas for 20 seconds. As the tip of the transfer tube approached the liquid withdrawal port on the tank, the port itself was purged with swiftly flowing helium gas and as the transfer tube actually entered the tank the purging line was removed from its other end. The transfer tube was then slowly lowered into the liquid helium tank and the helium dewar simultaneously. With the transfer tube seated securely, the gas phase withdrawal valve on the tank was opened and mated with the helium purging line (with gas still flowing). Then, using the main control valve on the helium gas purging tank, the pressure applied to the

surface of the liquid helium was adjusted to around 3.5 psi as indicated by the gauge on the liquid helium tank. As soon as the liquid helium was seen to be condensing in the inner dewar (generally after 2 or 3 minutes) the pressure was reduced to 2.25-2.5 psi for the duration of the transfer. The valve on helium gas tank was closed completely about one minute before the transfer was to end.

At that time, the transfer tube was slowly lifted until it first cleared the dewar top (and the top was plugged) and then cleared the liquid tank top (and the liquid withdrawal valve was closed). Then the sample was transferred from the liquid nitrogen bath and inserted in the helium dewar and the dewar was lowered into the sample compartment. For 1.4^{o}K experiments a vacuum pump was attached to the port on the inner dewar. Provision was made for introducing helium gas into the vacuum manifold to facilitate breaking the vacuum to change samples.

With the sample then in or near the exciting light beam, the next step was to optimize the sample position with respect to both the excitation and detection paths so as to obtain maximum phosphorescence. A second quartz lens focused the emission onto the entrance slit of the detection monochromator.

Emission Detection System. Emission from the sample was analyzed with a high intensity visible grating monochromator (Bausch and Lomb model 33-86-25-02) with a dispersion of 64 Angstroms per millimeter and blazed at 5000 Angstroms. The proper entrance slit width/exit slit width ratio was maintained at 1.7/1.0 as recommended by the manufacturer to give maximum spectral purity and the monochromator was fitted with a synchronous motor (Cramer model 1401, 2 rph) for scans at a rate of

4 Angstroms per second. A 1P28 photomultiplier tube with a cathode voltage of -1000 volts was used to detect emission from the sample and its output was fed into a sensitive electrometer for amplification. The electrometer was designed and built by Mr. Gerald O'Brien of the Chemistry department's electronics shop.

The output of the electrometer was fed into an X-Y recorder (Houston Instruments model 6520 with model 6800 analog adapter) so that a permanent record of spectra could be obtained. An event marker was used in conjunction with the recorder so that precise wavelength markings could be made on each spectrum while it was being recorded.

Phosphorescence Quantum Yields

Determination of the phosphorescence quantum yield of solid SO_2 required comparison of the SO_2 phosphorescence spectrum with phosphorescence spectra of substances having well-documented quantum yields with all spectra being obtained under precisely the same optical conditions. The sample under investigation and the reference standards were prepared to have identical optical densities at the excitation wavelength. All quantum yields were corrected for differences due to refractive indices (29).

Two reference standards were selected. They were benzophenone in EPA which is a rigid glass at 77°K and anthracene in ethanol which is a cracked glass at 77°K and more closely approximates the physical state of solid SO_2.

Fluorescence grade anthracene dissolved in ethanol was selected to minimize any problems that might arise due to large differences in refractive indices since the refractive index of ethanol is very close

to that calculated for solid SO_2. Two precautions must be taken when using anthracene, however. First, anthracene's 0-0 bands for absorption and emission overlap and all spectra must be corrected for self-absorption of the 0-0 band (29,31). Also, oxygen strongly quenches emission and the solution must be deoxygenated prior to use by bubbling nitrogen through it (31).

Quantum yield instrumentation was identical to that used for phosphorescence spectra except that the excitation monochromator was not used.

Phosphorescence Lifetimes

Measurement of phosphorescence lifetimes required a slightly different arrangement of the apparatus than was used for obtaining spectra. The changes were:

1. the continuous light source was replaced with a flashing source,
2. the interference filter was replaced with a color glass filter,
3. a color glass filter was inserted in the detection path,
4. and, a resistive load amplifier was used.

An electronic stroboscope (General Radio Strobotac model 1531-AB) provided a pulsed light source to study the decay of phosphorescence emission from the sample. The duration of the flash varied with the pulsing rate but was always maintained at a value (110 rpm) such that the lifetime of the flash was much smaller than the lifetime of the sample. Since the stroboscope was a much weaker light source than the continuous sources, it was necessary to replace the 3650 Angstrom

interference filter with a combination of higher transmission filters which would effectively eliminate scattered light. A UV transmitting/ visible absorbing color glass filter (Corning #7-39) with 50 percent transmission at 3670 Angstroms was placed between the excitation monochromator and the sample and a sharp cut yellow color glass filter (Corning #3-74; 60 percent transmission at 4250 Angstroms, 0 percent transmission at 3670 Angstroms) was placed between the sample and the detection monochromator.

When determining phosphorescence lifetimes it was essential that the high gain/slow response electrometer be replaced with a rapidly responding amplifier. For this application a resistive load type amplifier was chosen. Although it provided much less gain (by a theoretical factor of 10,000) than the electrometer, it gave a very satisfactory combination of gain and rapid response. A table of RC lifetimes is presented in Appendix I.

The output of the resistive load amplifier was fed into a Tektronix dual trace storage oscilloscope model 564B. Several decay traces were recorded on a single Polaroid photograph by making a time exposure with the model C-27 Polaroid camera attachment. Intensity versus time data was taken from the photographs, averaged, and entered into a FORTRAN least squares curve-fitting program which calculated the phosphorescence lifetime and then plotted the observed data versus the points calculated by the least squares program. The plotting program was written in APL by Mr. Rand Childs of the Chemistry department. Both programs are presented in Appendix II.

The decay data obtained at 1.4°K was not exponential like the data obtained at 77°K and 4.2°K and could not be analyzed with the FORTRAN and APL programs. A program written in BASIC and designed to extract the exponential components from a non-exponential curve was used (30). This program is presented in Appendix 2.

CHAPTER III

RESULTS

Phosphorescence Emission Spectrum of Solid $S^{16}O_2$ And $S^{18}O_2$ At 77°K

The phosphorescence emission spectrum of solid SO_2 has been analyzed by Hochstrasser and Marchetti (23) and we reexamined the spectrum as a first step in this research in order to authenticate our samples and methods. A typical phosphorescence emission spectrum measured in our laboratory at 77°K for $S^{16}O_2$ is presented in Figure 4. The 0-0 band maxima are presented in Table 1 and within reasonable experimental error (i.e. 10 Å) agree with the value of 3800.5 Å from Hochstrasser and Marchetti.

The band maxima for the phosphorescence spectrum of both $S^{16}O_2$ and $S^{18}O_2$ together with their associated assignments are found in Table 2. All observable bands involve combinations and/or overtones of ν_1 and ν_2. Bands involving the asymmetric vibration ν_3 are either very weak or absent.

Since all phosphorescence originates in the zeroth vibrational level of the triplet state and because of the mass effect upon the spacing of the vibrational levels in the ground state it would be expected that the spacings between the band maxima in the phosphorescence spectrum of $S^{18}O_2$ (termed $\Delta\nu^{18}$) would be less than the corresponding values of $\Delta\nu^{16}$. This trend is indeed present in Table 2 and serves as added verification of the difference between the two samples.

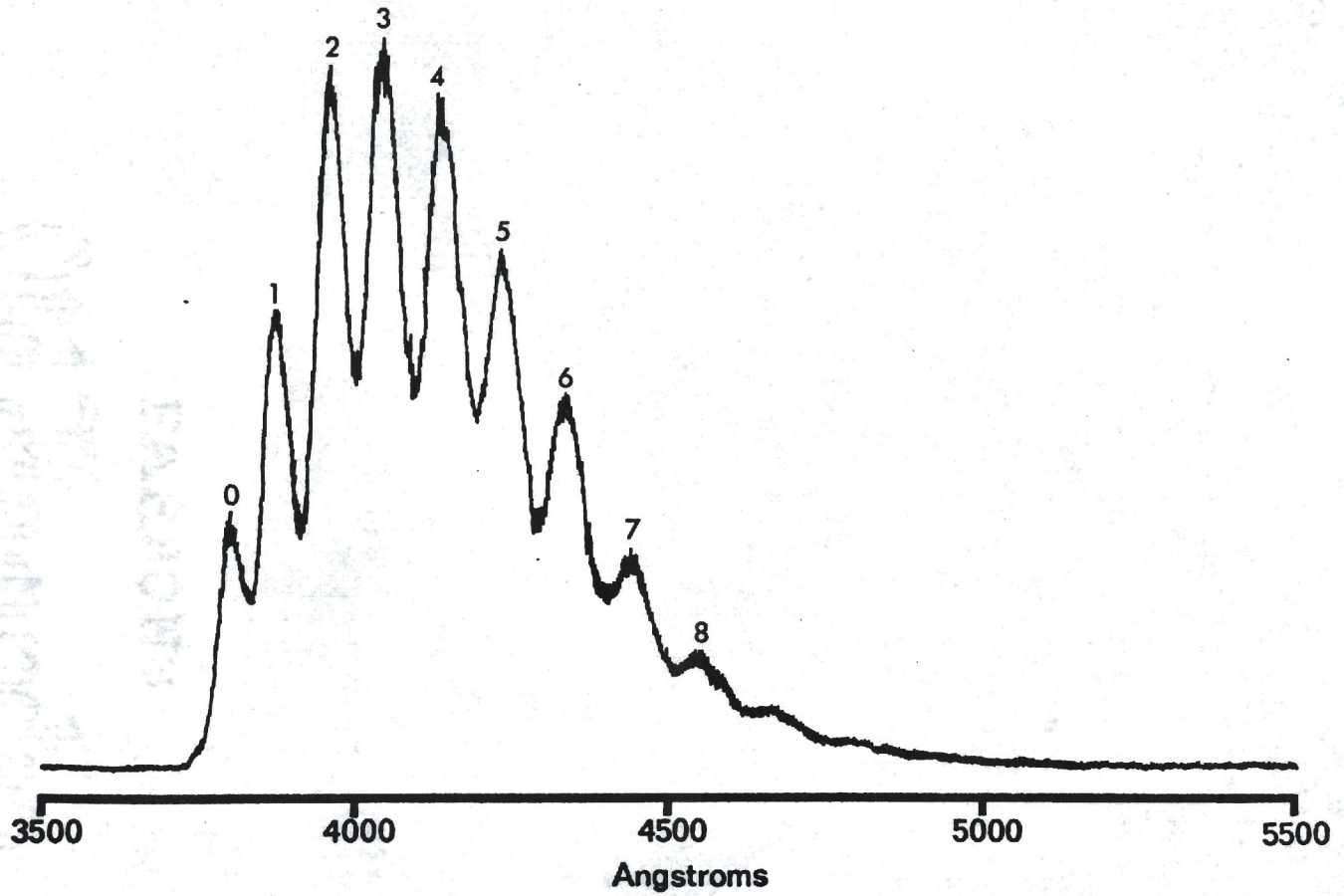

Fig. 4. Phosphorescence Emission Spectrum of Solid $S^{16}O_2$ at 77°K.

Table 1. 0-0 Band Maxima in the Phosphorescence Emission Spectrum of Solid $S^{16}O_2$ and $S^{18}O_2$ at 77°K.

Temperature	Compound	Band Maximum, Å [a]	Band Maximum, cm^{-1} [b]
77°K	$S^{18}O_2$	3806	26267
77°K	$S^{16}O_2$	3806	26267
4.2°K	$S^{16}O_2$ [c]	3800.5	26305

[a] Believed to be accurate within 10 Å. Error derives from reading of band maxima (5 Å) and from calibration of monochromator (5 Å).

[b] Vacuum cm^{-1}. See reference 50.

[c] See reference 23.

Table 2. Band Maxima in the Phosphorescence Emission Spectrum of Solid $S^{16}O_2$ and $S^{18}O_2$ at 77°K. [a]

Band Number	$\Delta\nu$, cm^{-1} [b,c]	$\Delta\nu^{16}$, cm^{-1} [d]	$\Delta\nu^{18}$, cm^{-1} [d]	Assignment
1	526	453	449	ν_2
2	1054	1038	1012	$2\nu_2$
3	1583	1577	1539	$3\nu_2$
4	2197	2178	2091	$\nu_1 + 2\nu_2$
5	2722	2715	2602	$\nu_1 + 3\nu_2$
6	3252	3254	3130	$\nu_1 + 4\nu_2$
7	----	3797	3645	
8	----	4367	4186	

[a] The 0-0 band is located at 3806 Å (26,267 cm^{-1}) and is identified as band number zero in Figure 4. All displacements are computed from there.

[b] Analysis by R. M. Hochstrasser and A. P. Marchetti (23) of the vibrational structure of the phosphorescence emission spectrum of solid $S^{16}O_2$ at 4.2°K gives $\nu_1 = 1149\ cm^{-1}$, $\nu_2 = 526\ cm^{-1}$, and $\nu_3 = 1330\ cm^{-1}$.

[c] Gas phase vibrational analysis gives $\nu_1 = 1151.4\ cm^{-1}$, $\nu_2 = 517\ cm^{-1}$, and $\nu_3 = 1361.8\ cm^{-1}$. See reference 23.

[d] Believed to be accurate within 40 cm^{-1}.

Table 3 presents the relative band intensities of $S^{16}O_2$ and $S^{18}O_2$ along with a band-by-band comparison. The 0-3 transition is the strongest in both spectra and after normalization to that band it is seen that the $S^{16}O_2$ emission is slightly but consistently stronger than that of $S^{18}O_2$.

Excitation Spectrum of Solid $S^{16}O_2$ and $S^{18}O_2$ at 77°K and 4.2°K

Band maxima in the excitation spectrum of $S^{16}O_2$ at 77°K and 4.2°K are presented in Table 4 together with the associated band spacings. The first two band spacings agree within about 15 percent but the 3282 Å band which is present in the 77°K is absent in the 4.2°K and no comparison can be made. A typical excitation spectrum for $S^{16}O_2$ at 77°K is presented in Figure 5.

Gas Phase Absorption Spectra of $S^{16}O_2$ and $S^{18}O_2$ in the 3800 Å Region at 298°K

An entire absorption spectrum for gaseous $S^{16}O_2$ as determined by Strickler and Howell (34) is given in Figure 6. The 2300 Å region has been assigned to a $^1B_2 \leftarrow {}^1A_1$ transition (21), the 3000 Å to a $^1B_1 \leftarrow {}^1A_1$ transition (22), and the 3800 Å region to a $^3B_1 \leftarrow {}^1A_1$ transition (20). Original plans for this research effort were to excite the SO_2 samples in either of the two very strong singlet-singlet absorption regions and then to depend upon intersystem crossing to populate the phosphorescent triplet state. It soon became evident that this was not a workable approach since the intersystem crossing rate constant was shown by Meyer, et al. (35) to be drastically temperature dependent and apparently approaching a zero value at 77°K and higher temperatures. Consequently it was decided to populate the triplet state directly by exciting the 3800 Å forbidden transition directly.

Table 3. Relative Band Intensities in the Phosphorescence Emission Spectrum of Solid $S^{16}O_2$ and $S^{18}O_2$ at 77°K. [a]

Band Number	Assignment	$S^{16}O_2$ Band Intensity	$S^{18}O_2$ Band Intensity	Intensity Ratio $\frac{I(S^{16}O_2)}{I(S^{18}O_2)}$
0	origin	0.3899	0.3283	1.16
1	ν_2	0.6307	0.6251	1.01
2	$2\nu_2$	0.9394	0.9315	1.01
3	$3\nu_2$	(1.0) [b]	(1.0) [b]	1.00
4	$\nu_1 + 2\nu_2$	0.9274	0.9313	1.00
5	$\nu_1 + 3\nu_2$	0.7635	0.7399	1.03
6	$\nu_1 + 4\nu_2$	0.5848	0.5237	1.10
7	------	0.4383	0.3337	1.28

a Based upon four spectra of each kind.

b All intensities normalized to that of band number four.

Table 4. Band Maxima in the Excitation Spectrum of Solid $S^{16}O_2$ at 77°K and 4.2°K.

Temperature	ν, Å	ν, cm^{-1} a	ν, cm^{-1} b	Intensity
77°K	3784	26420	0	strong
	3709	26954	534	strong
	3662	27300	880	strong
	3282	30460	4040	medium
4.2°K	3784	26420	0	medium
	3719	26881	461	medium
	3650	27389	969	strong

a Vacuum wave numbers believed to be accurate within 70 cm^{-1}.

b Vacuum wave numbers believed to be accurate within 20 cm^{-1}.

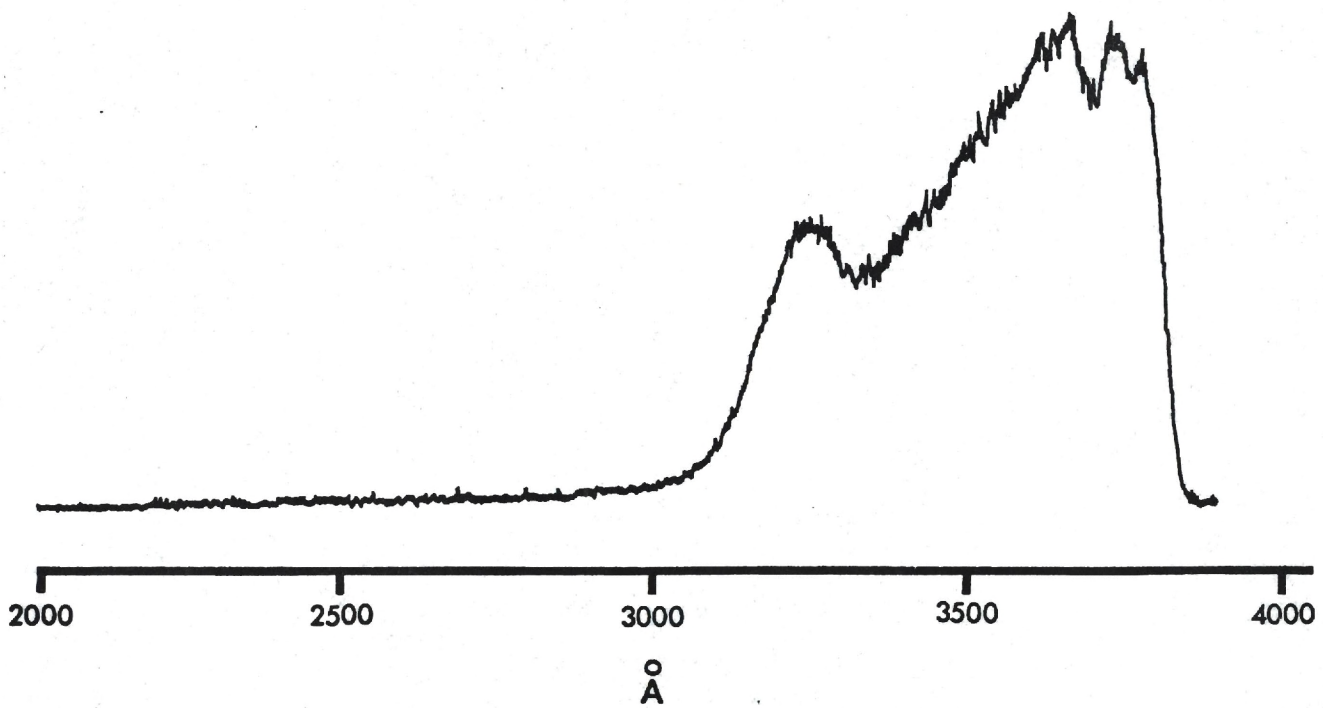

Fig. 5. Excitation Spectrum of Solid $S^{16}O_2$ at 77°K.

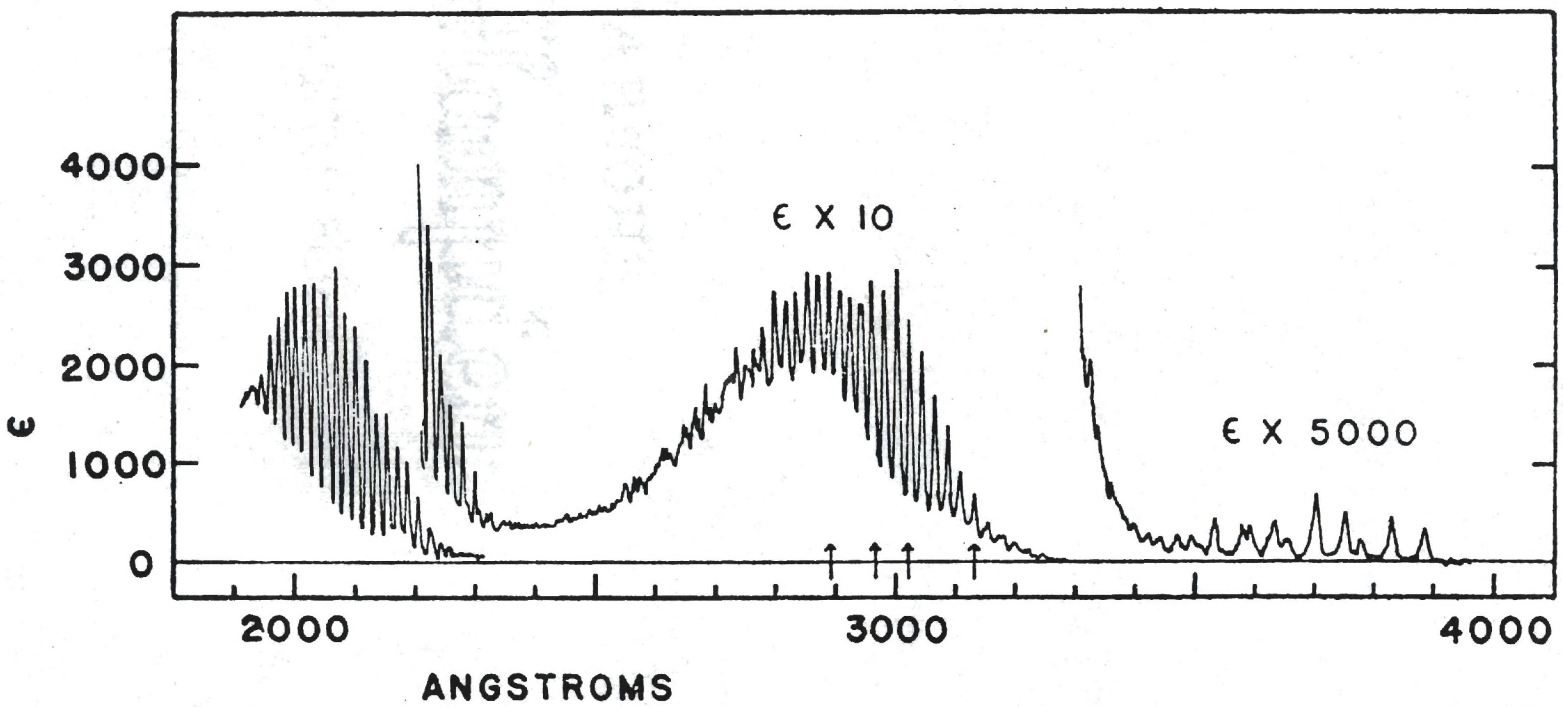

Fig. 6. Gas Phase Absorption Spectrum of $S^{16}O_2$ at 298°K.

As a preliminary step, the 3800 Å region of the gas phase absorption spectrum was studied at 298°K for both $S^{16}O_2$ and $S^{18}O_2$. Figure 7 shows this region for the $S^{18}O_2$ sample. Table 5 presents the relative band intensities and (in contrast to the phosphorescence emission spectrum) the $S^{16}O_2$ bands are generally weaker than the corresponding bands of $S^{18}O_2$. Table 6 shows the band maxima of the 3800 Å region and their associated spacings.

There was a possibility that Beer's law might not apply satisfactorily to the dilute gas samples used in this study (27) and so the optical density of the strongest band of the $S^{16}O_2$ 3800 Å absorption region (located at 27,000 cm^{-1}) was plotted as a function of concentration for five different concentrations. This data is presented in Figure 8 and it is seen that Beer's law is indeed valid up to a concentration of at least 0.03 moles per liter. All comparisons hereinafter mentioned between the gas phase absorption spectra of $S^{16}O_2$ and $S^{18}O_2$ are based upon data gathered in the region where there were no apparent deviations from Beer's law.

Quantum Yields of Phosphorescence for Solid SO_2 at 77°K and 4.2°K

The purpose of the quantum yield determinations was to give additional information as to the exact mechanism of any observed isotope effect. A change in the phosphorescence lifetime of a molecule is the most obvious manifestation of an isotope effect, but when lifetime data can be coupled with quantum yield data it becomes possible to partition the isotope effect into separate effects upon the two components of the phosphorescence decay which are termed the radiative and nonradiative rate constants. Unfortunately, quantum yields are

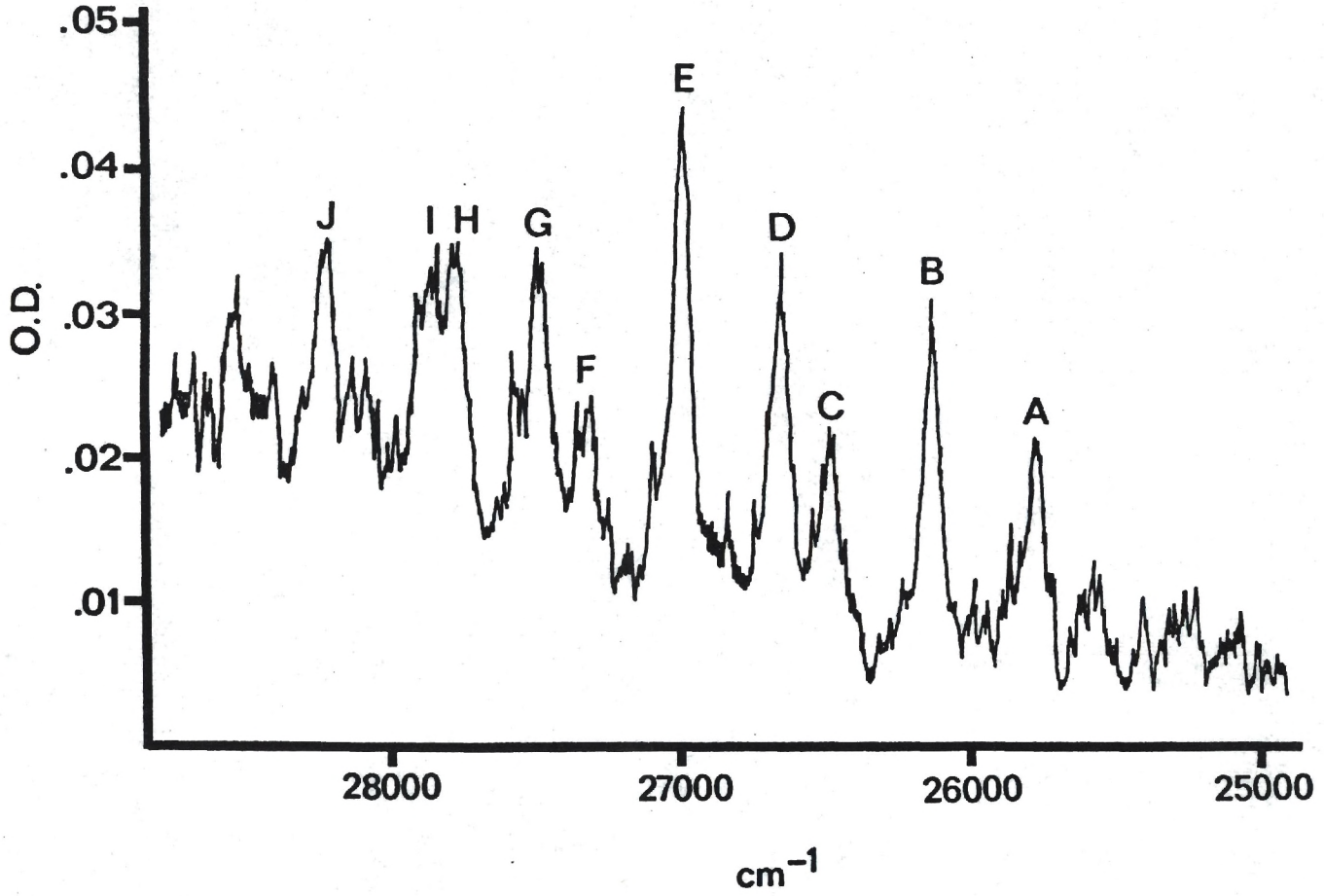

Fig. 7. Gas Phase Absorption in the 3800 Å Region of $S^{16}O_2$ at 298°K.

Table 5. Relative Band Intensities in the 3800 Å Region of the Gas Phase Absorption Spectra of $S^{16}O_2$ and $S^{18}O_2$ at 298°K. [a]

Band Designation	$S^{16}O_2$ Band Intensity	$S^{18}O_2$ Band Intensity	Intensity Ratio, $\frac{I^{16}}{I^{18}}$
I	0.5657	0.6691	0.85
H	0.5202	0.6642	0.78
G	0.6625	0.9901	0.67
F	0.2163	0.3217	0.67
E	(1.0) [b]	(1.0) [b]	1.0
D	0.7256	0.6074	1.2
C	0.3754	0.4605	0.82
B	0.5732	0.6790	0.84
A	0.4318	0.4420	0.98

[a] Based upon four spectra of each kind.

[b] All intensities normalized to that of band number 4.

Table 6. Band Maxima in the 3800 Å Region of the Gas Phase Absorption Spectrum of $S^{16}O_2$ and $S^{18}O_2$ at 298°K.

Band Designation	Assignment[e] v_1'	v_2'	v_3'	v_1''	v_2''	v_3''	$\Delta\nu^{16}$, cm^{-1} [a]	$\Delta\nu^{16}$, cm^{-1} [b,c]	$\Delta\nu^{18}$, cm^{-1} [b,d]
A	0	0	0	0	0	0	origin	origin	origin
B	0	1	0	0	0	0	356	350	360
C	0	2	0	0	0	0	736	638	700
D	1	0	0	0	0	0	920	900	880
E	1	1	0	0	0	0	1280	1250	1210
F	0	2	1	0	0	0	1635	1600	1490
G	2	0	0	0	0	0	1786	1760	1730
H	2	1	0	0	0	0	2120	2060	2010
I	0	1	2	0	0	0	2225	2170	2090
J	2	0	1	0	0	0	2558	2560	2450

[a] Unpublished data of R. M. Hochstrasser and A. P. Marchetti.

[b] Believed to be accurate within 2 cm^{-1}.

[c] Displacements are computed from the 0-0 band located at 25708 cm^{-1}.

[d] Displacements are computed from the 0-0 band located at 25770 cm^{-1}.

[e] See reference 52.

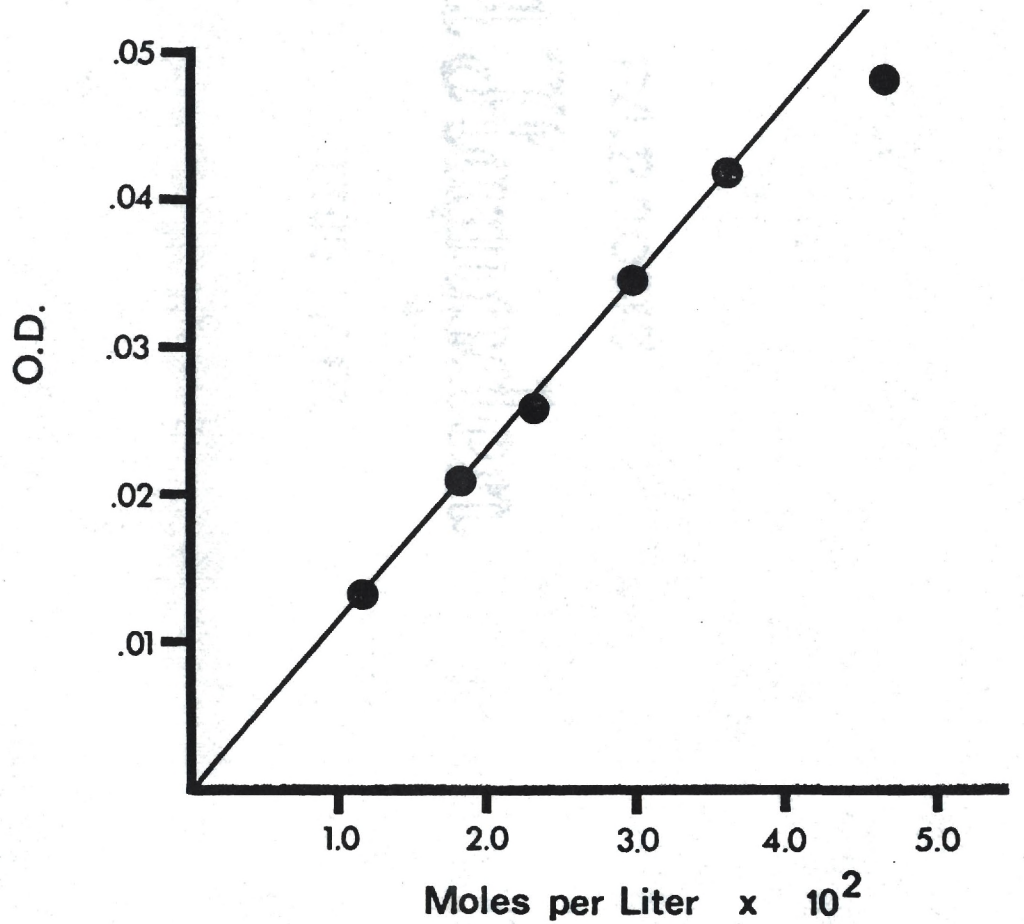

Fig. 8. Optical Density of the 27000 cm^{-1} Band of the Gas Phase Absorption Spectrum of $S^{16}O_2$ at 298°K Versus Concentration.

difficult to measure with high precision (31) and even though there may be a dramatic isotope effect upon the phosphorescence lifetime (which has been measured with good precision) it may be difficult to make a definitive statement concerning whether the radiative rate or the non-radiative rate has been most changed by the isotopic substitution.

The quantum yield of phosphorescence for solid SO_2 at 77^oK was determined relatively by comparison with two accepted quantum yield standards in hopes of minimizing any errors. The agreement between the two determinations was surprisingly good and results are presented in Table 7 with additional details concerning the method available in Appendix III.

Due to vast differences between sample geometries for 77^oK studies (where the sample is contained in a small dewar) and 4.2^oK studies (where the large helium dewar is used), a meaningful comparison between the quantum yield of a standard substance at 77^oK and its yield at 4.2^oK was impossible. Therefore the values for the quantum yield of SO_2 at 4.2^oK given in Table 7 are calculated on the assumption that the quantum yields of the standards have not changed with cooling from 77^oK to 4.2^oK. It is pointed out later in this section that k_{nr} (the non-radiative rate constant) decreases drastically with temperature and consequently the quantum yield increases. If this trend continues between 77^oK and 4.2^oK (and it probably does; see references 44 and 51) it is possible that the quantum yields of the standards could have increased at 4.2^oK (44,51), the 4.2^oK quantum yields for solid SO_2 may be larger than those presented in Table 7. Consequently, the 4.2^oK values in the table should be considered the very minimum values.

Phosphorescence Lifetimes for Solid $S^{16}O_2$ and $S^{18}O_2$ at 77°K and 4.2°K

A typical phosphorescence decay curve is presented in Figure 9 and graphs of log intensity versus time for both 77°K and 4.2°K are given together in Figure 10. The pronounced increase in the phosphorescence lifetime upon cooling from 77 K to 4.2 K is quite evident. The data at both temperatures is seen to be exponential over at least three lifetime periods.

A summary of the phosphorescence lifetimes for both $S^{16}O_2$ and $S^{18}O_2$ at 77°K and 4.2°K is given in Table 8 and the supporting data are presented in Appendices IV and V. The lifetime at 77°K for $S^{16}O_2$ of 0.99 msec does not compare favorably with the only other published value of 0.5 msec (36). The value of 0.5 msec is of questionable credibility, however, since the chopped light source used to excite the sample had a decay time of 0.3 msec or about 60 percent of the reported lifetime value. The light source used in our laboratory had a lifetime equal to approximately 1/2000 of the sample lifetime and consequently contamination of the sample decay by the decay of the exciting light source was eliminated. The lifetime for $S^{16}O_2$ at 4.2°K of 8.68 msec lies between the two published values of 7.5 ± 0.3 msec (33) and 9.6 ± 1 msec (35).

It should be noted that the magnitude of the oxygen-18 isotope effect is 29 percent at 77°K (with an experimental uncertainty of 11 percent) and that the magnitude decreases at 4.2°K to 12 percent (where the average experimental uncertainty is 2.7 percent). An accepted statistical test for determining whether two sets of data differ from each other with respect to some property or variable is

Table 7. Quantum Yield of Phosphorescence for Solid SO_2 at 77°K and 4.2°K.

Standard	77°K	4.2°K
Anthracene in ethanol	0.085 ± 0.004	0.625 ± 0.06 [a]
Benzophenone in cyclohexane	0.090 ± 0.004	0.575 ± 0.06 [a]

[a] This value may be larger than indicated. See text.

Table 8. Phosphorescence Lifetimes of Solid $S^{16}O_2$ and $S^{18}O_2$ at 77°K and 4.2°K.

Temperature	$\tau_p(S^{16}O_2)$, msec	$\tau_p(S^{18}O_2)$, msec	$\frac{\tau_p(S^{18}O_2)}{\tau_p(S^{16}O_2)}$
77°K	0.99 ± 0.11 (132 traces)[a]	1.28 ± 0.14 (126 traces)[a]	1.29
4.2°K	8.68 ± 0.14 (60 traces)[a]	9.73 ± 0.37 (36 traces)[a]	1.12

[a] Six decay traces were stored on each photograph and then analyzed together.

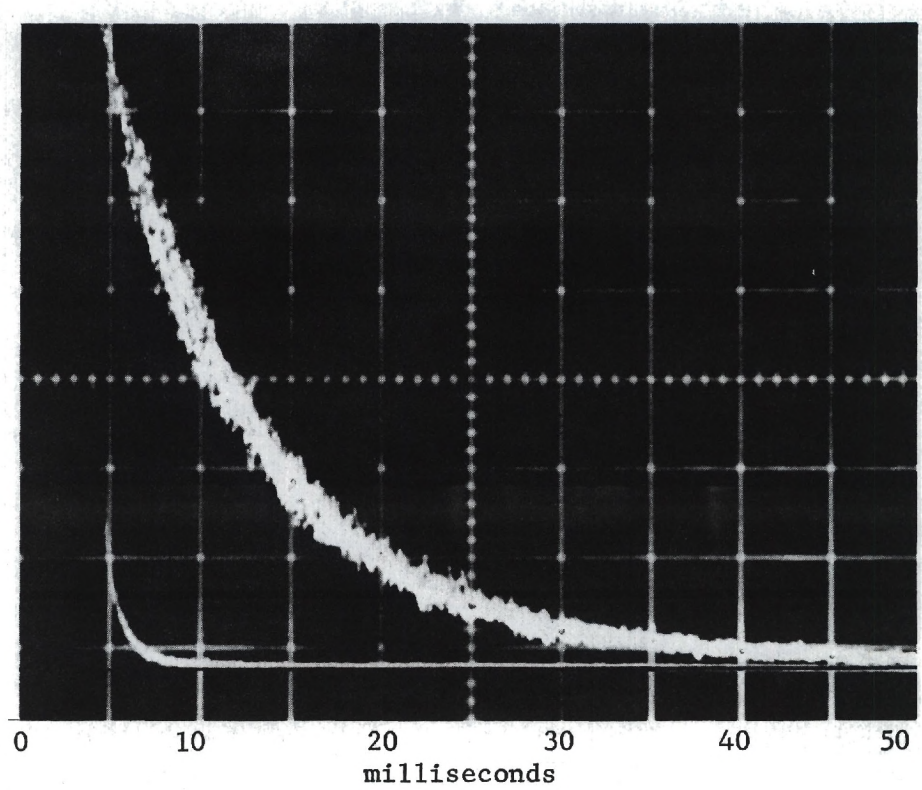

Fig. 9. Phosphorescence Decay Curve for Solid $S^{16}O_2$ at 4.2°K.

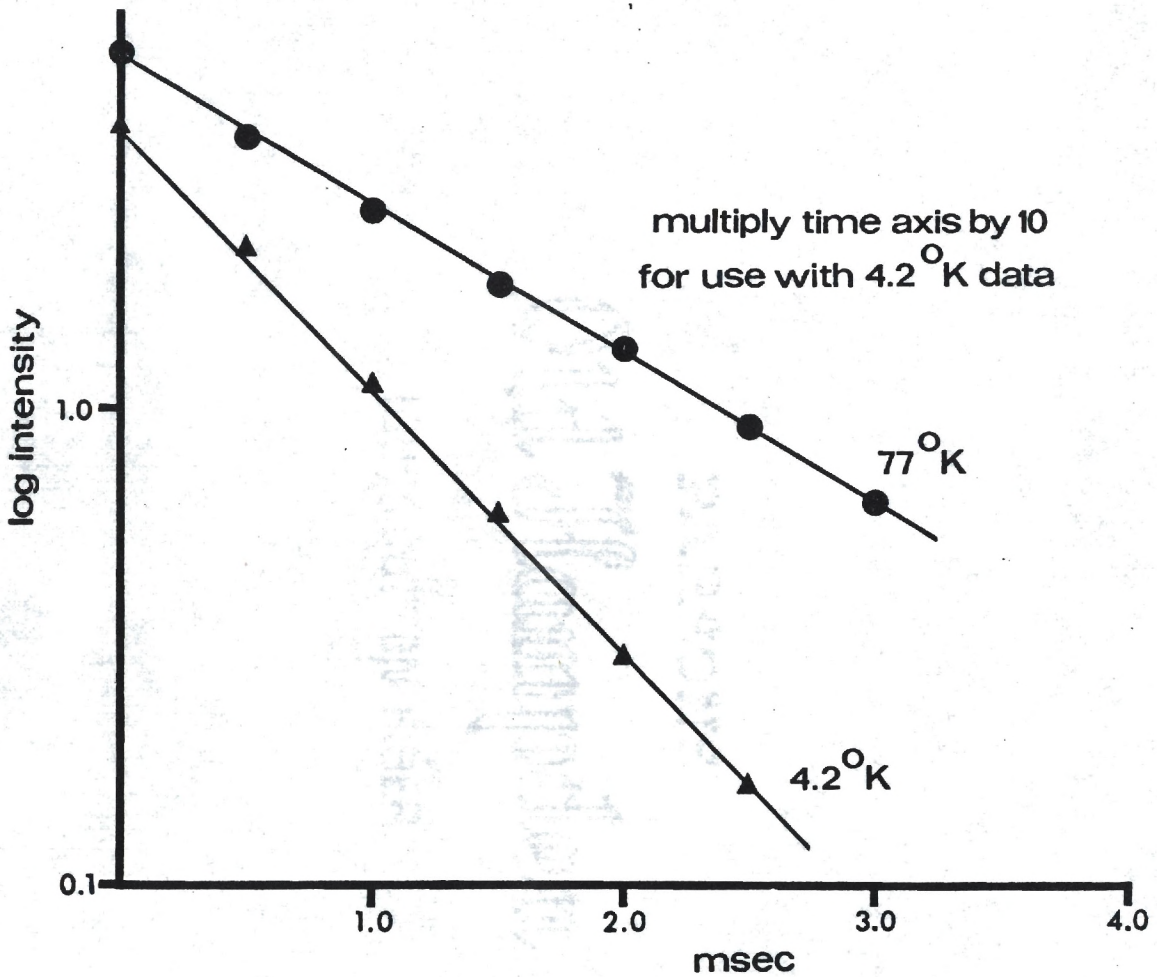

Fig. 10. Log Intensity Versus Time for the Phosphorescence Decay of Solid $S^{16}O_2$ at 77°K and 4.2°K.

"Student's t" test. Application of this test to the 77°K lifetime data predicts that we can state, with a probability of 98 percent of being correct, that the isotope effect is indeed significant. The confidence level increases to 99 percent for the 4.2°K data thereby demonstrating that the effect of isotopic substitution at both temperatures is indeed a real effect.

Radiative Rate Constants and Nonradiative Rate Constants for Solid $S^{16}O_2$ and $S^{18}O_2$ at 77°K and 4.2°K

Radiative rate constants (k_r) and nonradiative rate constants (k_{nr}) can be determined once suitable quantum yield data and phosphorescence lifetime data are obtained. The method of calculation of these rate constants is given in Appendix VI. Table 9 presents values of the radiative rate constants for both solid $S^{16}O_2$ and $S^{18}O_2$ at 77°K and 4.2°K and Table 10 gives the associated nonradiative rate constants. The most striking points to note are that the nonradiative rate constants are larger than the radiative rate constants by a factor of nearly ten at 77°K but at 4.2°K they become almost equal; and secondly, that the radiative rate constants show almost no variation with temperature while the nonradiative rate constants change by a factor of up to 20.

Phosphorescence Lifetimes of Solid $S^{16}O_2$ and $S^{18}O_2$ at 1.4°K

The phosphorescence lifetimes for solid $S^{16}O_2$ and $S^{18}O_2$ at 1.4°K are summarized in Table 11 where they are compared with the measurements of Tinti (33) and the supporting data is presented in Appendix VII. Three lifetimes are given for each sample because at 1.4°K the populations of

Table 9. Radiative Rate Constants (k_r) for Solid $S^{16}O_2$ and $S^{18}O_2$ at 77°K and 4.2°K.

Temperature	$k_r(S^{16}O_2)$ msec^{-1}	$k_r(S^{18}O_2)$ msec^{-1}	$\frac{k_r(S^{16}O_2)}{k_r(S^{18}O_2)}$
77°K	0.089 ± 0.014	0.069 ± 0.011	1.3
4.2°K	0.069 ± 0.008	0.062 ± 0.009	1.1

Table 10. Nonradiative Rate Constants (k_{nr}) for Solid $S^{16}O_2$ and $S^{18}O_2$ at 77°K and 4.2°K.

Temperature	$k_{nr}(S^{16}O_2)$ msec^{-1}	$k_{nr}(S^{18}O_2)$ msec^{-1}	$\frac{k_{nr}(S^{16}O_2)}{k_{nr}(S^{18}O_2)}$
77°K	0.922 ± 0.125	0.713 ± 0.099	1.3
4.2°K	0.046 ± 0.010	0.041 ± 0.012	1.1

Table 11. Phosphorescence Lifetimes of Solid $S^{16}O_2$ and $S^{18}O_2$ at 1.4°K.

	τ_1, msec	τ_2, msec	τ_3, msec	τ_1: τ_2: τ_3
$S^{16}O_2$ [a]	1.30 ± 0.05	6.8 ± 0.5	35.9 ± 1.2	1:5:28
$S^{16}O_2$ [b]	2.4 ± 0.1	12 ± 1	42 ± 2	1:5:18
$S^{18}O_2$ [c]	1.7 ± 0.3	5.6 ± 0.3	59.4 ± 6.9	1:3:35

[a] 24 decay traces (6 traces per photograph) were analyzed.

[b] See reference 33.

[c] 30 decay traces (6 traces per photograph) were analyzed.

the three spin states have no opportunity to equilibrate before they emit. This produces a non-exponential decay curve (see Figure 11) and an associated nonlinear plot of log intensity versus time (see Figure 12). The technique used to extract the three components of the decay curve is presented in Appendix II together with the computer programs used for the analysis.

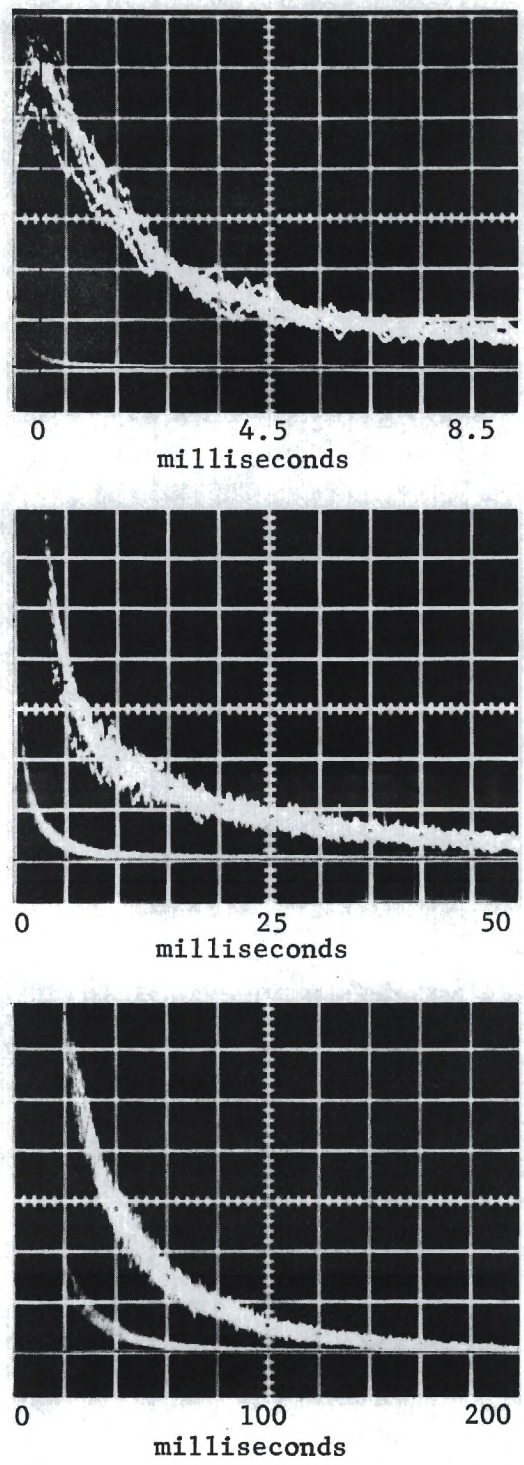

Fig. 11. Phosphorescence Decay Curve for Solid $S^{16}O_2$ at 1.4°K.

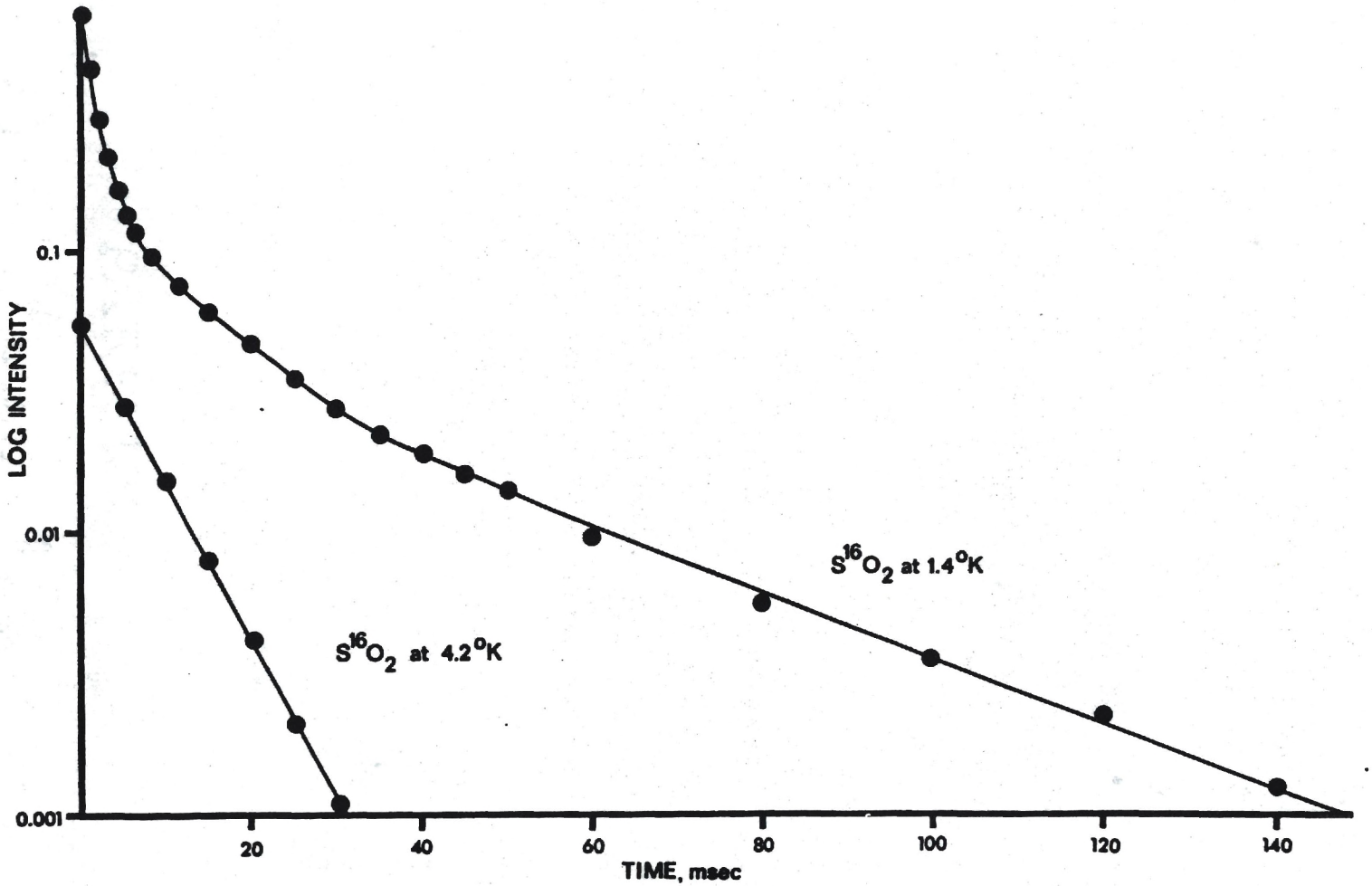

Fig. 12. Log Intensity Versus Time for the Phosphorescence Decay of Solid $S^{16}O_2$ at 1.4°K and at 4.2°K.

CHAPTER IV

DISCUSSION

Phosphorescence Emission Spectrum of Solid $S^{16}O_2$ and $S^{18}O_2$ at 77°K

As was shown in Table 2, the spacings between the band maxima in the phosphorescence spectrum of $S^{18}O_2$ (termed $\Delta\nu^{18}$) were observed to be less than the corresponding values of $\Delta\nu^{16}$. This is explained by recalling that the effect of substituting oxygen-18 in $S^{16}O_2$ will be to decrease the spacing of vibrational levels in all electronic states of the molecule. Since all phosphorescence originates in the zeroth vibrational level of the triplet state (44), it is only the changes in the spacing of vibrational levels in the $^1A_1$ ground state which could have any effect upon the phosphorescence spectrum.

Excitation Spectrum of Solid $S^{16}O_2$ and $S^{18}O_2$ at 77°K and 4.2°K

Excitation spectra provide useful information in that as the wavelength of the exciting light (with its quantum intensity kept constant) is varied through the singlet-triplet absorption region, the phosphorescence (from an optically dilute sample) will be proportional to the extinction coefficient of the singlet-triplet absorption. Therefore, the phosphorescence excitation spectrum will have the same shape as the singlet-triplet absorption spectrum and comparisons between the two can be made.

The 0-0 bands obtained in excitation spectra of solid $S^{16}O_2$ at 77°K and 4.2°K compare favorably with that obtained in the study of

the absorption spectrum of solid $S^{16}O_2$ at 4.2°K (23). The value from the excitation spectra is 26427 cm^{-1} (for both 77°K and 4.2°K) as compared with the absorption value of 26385 cm^{-1}. These values agree within the estimated experimental error of 70 cm^{-1}.

Gas Phase Absorption Spectra of $S^{16}O_2$ and $S^{18}O_2$ in the 3800 Å Region at 298°K

The value for the 0-0 band absorption maximum for $S^{16}O_2$ at 298°K obtained in this research (25708 cm^{-1}) agrees within experimental error (50 cm^{-1}) with the value of 25750 cm^{-1} reported by Merer (39).

An interesting observation is that the 0-0 band maximum of the emission spectrum (26269 cm^{-1}) for solid $S^{16}O_2$ at 77°K lies about 75 cm^{-1} to lower energies than the 0-0 band maximum for absorption of solid $S^{16}O_2$ at 4.2°K which is located at 26385 cm^{-1} (23). It has been suggested (23) that this offset arises because of the formation of local structural deformations of the crystal lattice in the environment of the excited molecule. In SO_2 this deformation results from a change in the electric dipole moment in going from the ground state to the excited state and from the accompanying change in the equilibrium geometry of the molecule.

A comparison of the 0-0 band maxima for the absorption spectra of $S^{16}O_2$ and $S^{18}O_2$ at 298°K shows that the 0-0 band for $S^{18}O_2$ lies 62 cm^{-1} to higher energies (i.e. 25770 cm^{-1}). This shift in band position can be attributed to the zero-point vibrations in the following manner (40). First, approximate the vibronic energy for the ground vibrational level of each electronic state as

$$E = E_{el} + E_{vib} = E_{el} + \sum_i \tfrac{1}{2} h\nu_i \, . \qquad (1)$$

Assuming a 0-0 transition (i.e. no excitation of vibrations) then the energy of the 0-0 transition is

$$\nu_{0-0} = E_u - E_1 + \tfrac{1}{2}\sum_i(\nu_u - \nu_1) \quad . \tag{2}$$

Therefore (assuming that the electronic energies are unchanged by isotopic substitution) the shift in the 0-0 transition is

$$\Delta\nu_{0-0} = \nu_{0-0} - \overset{i}{\nu}_{0-0} = \tfrac{1}{2}\sum_i(\nu_u - \nu_1) - \tfrac{1}{2}\sum_i(\overset{i}{\nu}_u - \overset{i}{\nu}_1) \quad . \tag{3}$$

The calculated value of this 0-0 band shift due to isotopic substitution is 28 cm^{-1}.

The ratio of the integrated absorption spectra in the 3800 Å region at 298°K showed the $S^{16}O_2$ spectrum to be more intense than that of the $S^{18}O_2$ by 32 percent. Knowing that one of the eventual goals of this research was to determine the effect of isotopic substitution upon the radiative and nonradiative relaxation rate constants of the $^3B_1$ state, the method of Strickler and Berg (41) was employed to calculate radiative rate constants for $S^{16}O_2$ and $S^{18}O_2$ at 298°K based upon the integrated singlet-triplet absorption spectrum. The equation is strictly applicable only to strong, allowed transitions but we were primarily interested in a qualitative comparison of the values rather than the absolute values themselves. The Strickler-Berg equation is as follows:

$$k_r = (8)(2303)\,\pi c \tilde{\nu}_{ul}^{\,2}\; n^2\; N^{-1}\; \frac{g_l}{g_u} \int \epsilon d\tilde{\nu} \qquad (4)$$

where

"u" represents the upper electronic state

"l" represents the lower electronic state

c = the speed of light in vacuum

$\tilde{\nu}_{ul}$ = the average frequency of the transition in cm^{-1}

n = the refractive index of the medium

N = Avogadro's number

g = degeneracy of the indicated electronic state, and

ϵ = the molar extinction coefficient.

The calculated values of the radiative rate constants are 0.13 ± 0.02 $msec^{-1}$ for the $S^{16}O_2$ spectra, 0.10 ± 0.01 $msec^{-1}$ for the $S^{18}O_2$ spectra, and the ratio of k_r^{16}/k_r^{18} equals 1.3.

Oscillator strengths were also calculated from the integrated singlet-triplet absorption spectra through use of the following equation (42):

$$f_i = 4.319 \times 10^{-9} \int \epsilon_i d\tilde{\nu} \quad . \qquad (5)$$

The following values were calculated:

$$f(S^{18}O_2) = 3.62 \times 10^{-7} \quad \text{and} \quad f(S^{16}O_2) = 4.80 \times 10^{-7}.$$

The only reported value for the oscillator strength of $S^{16}O_2$ in the 3800 Å region is that of 1.7×10^{-7} determined by Coon in 1958 (47).

Phosphorescence Lifetimes of Solid $S^{16}O_2$ and $S^{18}O_2$ at 77°K and 4.2°K

As was mentioned in the Results section, at 77°K the solid $S^{18}O_2$ sample had a phosphorescence lifetime which exceeded that of the $S^{16}O_2$ sample by a factor of 1.29. This was shown to be a significant difference by application of "Student's t" test which gave a confidence level of 98 percent to the conclusion that the isotope effect was indeed a real effect. A 12 percent effect was noted at 4.2°K and the effect was significant with a confidence level of 99 percent.

Phosphorescence Lifetimes of Solid $S^{16}O_2$ and $S^{18}O_2$ at 1.4°K

A triplet state is an electronic state in which there are two electrons with unpaired spins. The degeneracy of the state equals (2S + 1) and is therefore threefold degenerate in the absence of a magnetic field with each of the three spin sublevels having a different component of spin angular momentum. When the three spin sublevels are subjected to a magnetic field (either externally applied from an electromagnet or internally applied as from spin-orbit coupling) the degeneracies are removed and three discrete spin sublevels are created. The magnitude of the splitting between the spin sublevels is typically just a few wavenumbers which is less than kT at normal observation temperatures. Initially, the spin levels may not be equally populated, but energy conversion (enhanced by spin-lattice-relaxation or SLR) takes place rapidly (ca. 10^{-5} sec at 80°K) and the levels equilibrate before emitting. At very low temperatures (i.e. 1.4°K) the SLR processes slow down drastically (ca. 0.1 sec) and the populations of the three sublevels may no longer be equal, but instead will depend upon the mechanism of triplet population and the rate of sublevel relaxation.

It has been shown that the average rate of decay for several such sublevels is equal to the sum of the individual decay rates (45), or mathematically

$$k_{avg} = \sum_{i=1}^{3} n_i k_i \qquad (6)$$

where n_i = the fraction of molecules decaying from state "i". Since

$$k_{avg} = (\tau_p)^{-1}, \qquad (7)$$

a simple substitution leads to

$$\tau_{avg} = \left(\sum_{i=1}^{3} n_i (\tau_i)^{-1}\right)^{-1} = 3(1/\tau_1 + 1/\tau_2 + 1/\tau_3)^{-1} \qquad (8)$$

which permits estimation of a high temperature (i.e. 4.2°K) lifetime with the assumption that SLR processes are fast relative to phosphorescence at 1.4°K. These predicted 4.2°K lifetimes as computed from our data are 3.2 msec for $S^{16}O_2$ and 3.8 msec for $S^{18}O_2$. The lifetimes we actually observed at 4.2°K were 8.68 msec and 9.73 msec for $S^{16}O_2$ and $S^{18}O_2$, respectively. Since the 4.2°K lifetimes are more than twice the shortest lifetime extracted at 1.4°K, τ_1 must be assigned as the dominant spin state (33). The magnitude of the isotope effect upon τ_1 at 1.4°K is very nearly the same as the observed effect upon the overall lifetime observed at 4.2°K (i.e. 3.8/3.2 approximately equals 9.73/8.68).

Radiative and Nonradiative Relaxation Rates of the $^3B_1$ State of Solid $S^{16}O_2$ and $S^{18}O_2$ at 77°K and 4.2°K

It should be clear, indeed, that the effect of isotopic substitution upon the phosphorescence lifetime of solid SO_2 is a significant one. At both 77°K and 4.2°K the magnitude of the lifetime lengthening exceeds the measured experimental uncertainty by at least a factor of three. In addition, careful application of an accepted statistical test to the data shows that the confidence level of the data is high with respect to the isotope effect being a real effect. It must be re-emphasized at this point, however, that accurate calculations of radiative and nonradiative rate constants depend upon both the accuracy with which phosphorescence lifetimes can be measured and upon the accuracy with which phosphorescence quantum yields can be determined. As a consequence, the partitioning of a given isotope effect into its separate effects upon the radiative and nonradiative rate constants can be a difficult procedure.

The first step in discerning the integrity of our data was to compare the radiative constants calculated from the integrated singlet-triplet absorption spectra of $S^{16}O_2$ and $S^{18}O_2$ by the method of Strickler and Berg (41) with those obtained by measurements of the phosphorescence lifetimes and quantum yields of solid $S^{16}O_2$ and $S^{18}O_2$ at 77°K and 4.2°K. Referring to Table 9 shows that the values obtained by the latter method gave $k_r(S^{16}O_2)/k_r(S^{18}O_2)$ ratios of 1.3 (at 77°K) and 1.1 (4.2°K) while the method of Strickler and Berg gave an entirely independent estimate of the same ratio equal to 1.3. This good agreement between ratios of radiative rate constants determined by two completely different methods serves to lend added support to the quality of our data.

One of the striking features of Table 10 is the marked temperature dependence of the nonradiative rate constants. Heller, Freed, and Gelbhart (46) have recently advanced a theory to explain this behavior. They contend that the observed rate will often exhibit an Arrhenius behavior with an average thermal activation energy which is termed E_A. Their suggested mechanism assumes that the activated barrier (E_A) arises from thermal vibrational excitation of the initially vibrationless state which corresponds to the nonradiative rate constant at zero temperature which is termed k_0. The equation to describe this observation is

$$k_{nr}^{obs}(T) = k_0 + k_1 \exp(-E_A/k_b T) \quad . \tag{9}$$

The activation energy was calculated with k_b taken as being equal to the gas constant "R" (1.987 cal/mole-^oK) and the values determined were:

$$E_A(S^{16}O_2) = 21 \text{ calories and } E_A(S^{18}O_2) = 16 \text{ calories.}$$

These values are equal within experimental error and are both on the order of 6 cm^{-1} which is of the same magnitude as a lattice vibration.

Reference to Tables 9 and 10 points up the fact that both the radiative rate constant (k_r) and the nonradiative rate constant (k_{nr}) show an isotope dependence. As was mentioned in the Introduction, it was hoped that this research effort could help further elucidate the coupling mechanism which gave allowed character to the otherwise spin-forbidden $^3B_1 \leftarrow\!\!- {}^1A_1$ transition. Brand, et al. (20), have reported that the $^3B_1 \leftarrow\!\!- {}^1A_1$ transition has two independent nonvanishing transition

moments and he concludes that spin-orbit coupling with the $^1B_2$ states (and with a probable secondary contribution from the $^1A_1$ states) is the important perturbation that lends intensity to the forbidden transition.

The isotope effect upon the nonradiative rate constants can arise either from the electronic matrix elements or, more often, from the Franck-Condon integrals which couple the vibrational wavefunctions of the triplet and ground singlet states. Due to the mass effect upon the spacing of vibrational levels in the electronic state, the vibrational level of the $^1A_1$ state in an $S^{18}O_2$ molecule which is isoenergetic with a low-lying vibrational level of the $^3B_1$ state will have a higher quantum number than the isoenergetic vibrational level of an $S^{16}O_2$ molecule. Consequently, the Franck-Condon integral will be smaller in the $S^{18}O_2$ case and the radiationless transition will be correspondingly slower.

However, for radiative transitions the Franck-Condon factors only dictate the distribution of intensity among the 0-0 transition and transitions to excited vibrational levels of the final electronic state and they have no effect on the overall integrated intensity. Therefore, the observed isotope effect on rates of radiative relaxation must be largely due to a mass effect upon the electronic matrix elements (49). Lim and Fischer (49) have reported four mechanisms for radiative singlet-triplet transitions, the first of which is not subject to an isotope effect. The four mechanisms are:

1. spin-orbit coupling only (no isotope effect expected),
2. spin-orbit coupling and Herzberg-Teller vibronic coupling (some isotope effect expected),

3. spin-orbit coupling and non-Born-Oppenheimer vibronic coupling (greater isotope effect expected), and
4. spin-orbit coupling and non-Born-Oppenheimer vibronic coupling (includes an additional non-Born-Oppenheimer term; greatest expected isotope effect).

The fortunate benefit of the treatment of this problem by Lim and Fischer is that the mechanism involved can be recognized experimentally if careful measurements are made. Mechanism two is characterized by the following relationship (where n = 1) between the radiative rate constants and the change in the fundamental vibrational frequencies due to isotope substitution (see Tables 12 and 13):

$$\frac{k_r(S^{16}O_2)}{k_r(S^{18}O_2)} = \left[\frac{(S^{16}O_2)}{(S^{18}O_2)}\right]^n \qquad (10)$$

Mechanism three is characterized by a similar experimentally recognizable quantity and only differing from the previous equation in that the right hand term is cubed (i.e. n = 3). Mechanism four is distinguished by the right hand term being raised to the fourth power (i.e. n = 4).

Table 12 presents a comparison between the ratios of the radiative rate constants and right hand term of equation (10) for the three coupling mechanisms of Lim and Fischer which can produce an isotope effect upon the radiative rate constant of the triplet state decay. It is seen that within experimental uncertainty any of the three mechanisms is plausible.

Tables 12 and 13 show that the average effect upon the three fundamental vibrational frequencies of $S^{16}O_2$ with oxygen-18 substitution is 4 percent i.e. $\frac{\bar{\nu}(S^{16}O_2)}{\bar{\nu}(S^{18}O_2)} = 1.04$

Table 12. Comparison of the Ratios of Radiative Rate Constants for Solid $S^{16}O_2$ and $S^{18}O_2$ at 77°K and 4.2°K With the Right Hand Term of Lim and Fischer's Equation.

77°K $\frac{k_r(S^{16}O_2)}{k_r(S^{18}O_2)}$	4.2°K $\frac{k_r(S^{16}O_2)}{k_r(S^{18}O_2)}$	Mechanism Number	Exponent of Right Hand Term in Equation 10	Value of Right Hand Term in Equation 10 [a]
1.29 ± 0.41	1.11 ± 0.29	2	1	1.04
		3	3	1.12
		4	4	1.17

[a] Refer to Table 13.

Table 13. Calculated Effect of Oxygen-18 Substitution in $S^{16}O_2$ Upon ν_1, ν_2, And ν_3 Assuming a Valence Force Field Model for the $^3B_1$ State.

	$S^{16}O_2$	$S^{18}O_2$	% Isotope Effect
ν_1, cm^{-1}	1142.2	1090.0	4.5
ν_2, cm^{-1}	528.2	506.6	4.1
ν_3, cm^{-1}	1377.5	1334.1	3.2
		Average =	3.9%

a
See reference 38.

b
Triplet state O-S-O angle of 126° 13' from reference 20.

CHAPTER V

CONCLUSIONS

1. Oscillator strengths for $S^{16}O_2$ and $S^{18}O_2$ were calculated from the integrated absorption spectra in the 3800 Å region at 298°K and were determined to be 4.80×10^{-7} and 3.62×10^{-7}, respectively, indicating that the $S^{16}O_2$ spectrum was more intense than the $S^{18}O_2$ spectrum by a factor of 1.32.

2. At 77°K, solid $S^{18}O_2$ was observed to have a phosphorescence lifetime of 1.28 msec while solid $S^{16}O_2$ had a phosphorescence lifetime of 0.99 msec.

3. At 4.2°K, solid $S^{18}O_2$ was observed to have a phosphorescence lifetime of 9.73 msec while the solid $S^{16}O_2$ had a phosphorescence lifetime of 8.68 msec.

4. At 1.4°K, where spin-lattice-relaxation is slow compared to phosphorescence, the uncertainty in the data was large, yet the phosphorescence lifetime of solid $S^{18}O_2$ was longer than that of solid $S^{16}O_2$ by a factor of 12 percent.

5. The quantum yield of solid SO_2 at 77°K was determined relative to two standards to be 0.087 ± 0.004 and at 4.2°K was determined to be no less than 0.60 ± 0.06.

6. The radiative and nonradiative relaxation rates of the $^3B_1$ state of solid $S^{16}O_2$ at 77°K and 4.2°K were observed to decrease with oxygen-18 substitution.

7. The nonradiative relaxation rates for the $^3B_1$ state of solid $S^{16}O_2$ and $S^{18}O_2$ were observed to be strongly temperature dependent and to decrease by a factor of 20 between 77°K and 4.2°K.

APPENDIX I

RC LIMITED DECAY TIMES

Load Resistance (in Ohms)	Gain	Minimum Lifetime
50	1	10 nanoseconds
100	2	0.2 microseconds
500	10	1.0 microseconds
1 K	20	2.0 microseconds
5 K	100	10.0 microseconds
10 K	200	2×10^{-5} seconds
50 K	1000	1×10^{-4} seconds
100 K	2000	2×10^{-4} seconds
500 K	10000	1×10^{-3} seconds
1000 K	20000	2×10^{-3} seconds

APPENDIX II

ANALYSIS OF MULTICOMPONENT DECAY CURVES

For a mixture of several independent exponential decays the result of plotting log intensity versus time is a concave upward curve. This curvature results because the contribution of the shorter-lived components becomes increasingly less as time passes. In fact, after a sufficiently long period of time the longest component will entirely predominate. If this last portion of the curve (which is a straight line since it represents only a single exponential decay) is extrapolated back to time=zero then the lifetime of the long component can be calculated. If this extrapolated line is then subtracted point-by-point from the original curve the new data points which result represent the decay of all components except the longest-lived one. The two-component curve is then treated in the same way again and the intermediate lifetime component is extracted. The remaining corrected data points are then plotted again and finally the shortest lifetime component is extracted.

In theory, any number of exponential components can be extracted in this manner but in practice experimental uncertainties make analysis of a three-component curve difficult, and even two-component curves may defy analysis if the components have lifetimes which differ by less than a factor of two (30).

In analysis of the 1.4^{o}K lifetime data presented herein, the data gathered at long times (and which determined τ_3) was the data

in which the signal-to-noise ratio was the smallest and consequently the uncertainty in the data the largest. Clearly, any error which is introduced by improper extraction of τ_3 can only propagate and lead to faulty values of τ_2 and τ_1.

The BASIC analysis program which performed a non-weighted least squares analysis of the data and the associated program which subtracted the extrapolated baseline from the remaining points is presented in Appendix II.

```
@TABSET,W 72
@ED,R LONG.JOHN
READ-ONLY MODE
ED 13.00-07/22-15:30-(43,)
EDIT
0:LNPRINT!


 1:        REWIND 7
 2:        WRITE (6,1)
 3:1        FORMAT(3X,'LEAST SQUARES EMISSION LIFETIME CALCULATION',I2,/)
 4:        DIMENSION X(20),Y(20) ,Z(20)
 5:        WRITE (6,3)
 6:3       FORMAT(1H,'NUMBER OF DATA SETS NN=')
 7:        READ (5,4)NN
 8:4       FORMAT()
 9:        K=1
10:        VARSLO=0.
11:        VARCEP=0.
12:        WRITE (6,5)
13:5       FORMAT(1H,'NUMBER OF DATA POINTS IN ALL SETS')
14:        READ (5,4) NO
15:        RNO=FLOAT (NO)
16:        WRITE (7,999) RNO
17:999     FORMAT(1PE13.7)
18:        WRITE (6,7)
19:  7     FORMAT (////,' ENTER YOUR TIME DATA FOR ALL TRACES')
20:        READ (5,4) (X(I),I=1,NO)
21:        DO 800 I=1,NO
22:800     WRITE (7,999)X(I)
23:        WRITE (6,8)
24:8       FORMAT (' YOUR TIME DATA READ AS FOLLOWS:',I2,/ )
25:        WRITE (6,4) (X(I),I=1,NO    )
26:52        WRITE (6,53)K
27:53      FORMAT(' ENTER YOUR TITLE FOR TRACE K= ',I2,/)
28:        READ (5,54)
29:54      FORMAT(40H                                              )
30:       WRITE(7,54)
31:        WRITE (6,9)K
32:9       FORMAT(' ENTER INTENSITY DATA FOR TRACE K= ',I2,/)
33:        READ (5,4) (Z(I),I=1,NO)
34:        DO 801 I=1,NO
35:        Y(I)=ALOG10(Z(I))
36:801      WRITE (7,999) Y(I)
37:        WRITE (6,10)
38:10      FORMAT (' YOUR INTENSITY DATA READ AS : ')
39:        WRITE (6,4) (Z(I),I=1,NO)
40:C       ALL DATA HAS NOW BEEN ENTERED AND CONFIRMED.
41:C       NOW, NORMALIZE THE INTENSITY DATA IF DESIRED.
42:C       DO 11 I=1,NO
43:C     YN(I)= Y(I)/Y(1)    MAKE THIS STMNT 11 TO USE
44:        SUMY=0.
45:        SUMX=0.
46:        XBAR=0.
47:        YBAR=0.
48:        SUMXY=0.
49:        SXSY=0.
```

```
    5:        SUMXSQ=0.
   51:         SUMYSQ=0.
   52:         DO 13 I=1,NO
   53:         SUMY=SUMY+Y(I)
   54:         SUMX=SUMX+X(I)
   55:         SUMXY=SUMXY+X(I)*Y(I)
   56:              SXSY=SXSY+(SUMX*SUMY)/NO
   57:         SUMXSQ=SUMXSQ+(X(I))**2
   58:13       SUMYSQ=SUMYSQ+(Y(I)**2)
   59:         XBAR=XBAR+SUMX/NO
   60:         YBAR=YBAR+SUMY/NO
   61:         SEXY= SUMXY-(SUMX*SUMY)/NO
   62:         SEXX= SUMXSQ-(SUMX**2)/NO
   63:         SLOPE= SEXY/SEXX
   64:         CEPT= YBAR-SLOPE*XBAR
   65:         WRITE (6,69) SLOPE
   66:         WRITE (6,70) CEPT
   67:69       FORMAT (' SLOPE= ',1PE13.7)
   68:70        FORMAT(' INTERCEPT= ',1PE13.7)
   69:         YSUMSQ=(SUMY**2.)/NO
   70:         XSUMSQ=(SUMX**2)/NO
   71:         SEYY=SUMYSQ-YSUMSQ
   72:         SEXQUO=(SEXY**2)/SEXX
   73:         A= ((SEYY-SEXQUO)/(NO-2))
   74:         SY= SQRT(A)
   75:         VARSLO=(SY**2)/SEXX
   76:         VARCEP=((SEYY-SEXQUO)/(NO-2))*((1/NO)+((XBAR**2)/SEXX))
   77:         D=0.
   78:         C=NO/((NO*SUMXSQ)-XSUMSQ)
   79:         DO 25 I=1,NO
   80:25       D=D+(((Y(I)-CEPT-SLOPE*X(I))**2)/NO)
   81:C        SDSLO= STD.DEV. FROM 3-82 IN PARRATT
   82:           SDSLO=(SQRT(C))*(SQRT(D))
   83:         WRITE (6,14) VARSLO
   84:         WRITE (6,15) VARCEP
   85:         WRITE (6,17) SDSLO
   86:          TAU=-1/(2.303*SLOPE)
   87:         WRITE (6,50) TAU
   88:50       FORMAT(' LIFETIME= ',1PE13.7,' MILLISECONDS')
   89:C         STDTAU IS THE STANDARD DEVIATION OF THE LIFETIME
   90:C         (STDTAU/TAU    =    SDSLO/SLOPE
   91:         STDTAU=(SDSLO/SLOPE)*TAU
   92:         WRITE(6,51) STDTAU
   93:51       FORMAT(' STD. DEVIATION IN LIFETIME= ',1PE13.7,///)
   94:17       FORMAT(' STD. DEVIATION OF SLOPE PER PARRATT 3-82 = ',1PE13.7)
   95:14       FORMAT (' ESTIMATED VARIANCE OF THE SLOPE= ',1PE13.7)
   96:15       FORMAT(' ESTIMATED VARIANCE OF THE INTERCEPT= ',1PE13.7)
   97:         WRITE (7,999) SLOPE
   98:         WRITE (7,999) CEPT
   99:         K=K+1
  100:         IF (K.LE.NN) GO TO 52
  101:         END FILE 7
  102:        END
SCAN:102
EOF:102
0:@EOF
NO CORRECTIONS APPLIED.
```

```
$FPLOTIT[¤]
   $F PLOTIT X ;J
[1]    'DATA' FIASGX 1
[2]    K$SCONVERT FIREAD 1
[3]    J$S1
[4]    K$SK-1
[5]    T$SCONVERT FIREAD 1
[6]   GET1:T$ST,CONVERT FIREAD 1
[7]    $G((J$SJ+1)$<K)/GET1
[8]   GO:J$S1
[9]    TITLE$SFIREAD 1
[10]   $G(1ΔTITLE=&1)/STOP
[11]   $¤
[12]   INT$SCONVERT FIREAD 1
[13]  GET2:INT$SINT,CONVERT FIREAD 1
[14]   $G((J$SJ+1)$<K)/GET2
[15]   S$SCONVERT FIREAD 1
[16]   I$SCONVERT FIREAD 1
[17]   NEW$SI+S#T
[18]   W$S0
[19]   W$S0
[20]   W$S0
[21]   ''
[22]   ($L(38-(0.5#$RTITLE)))$R' ';TITLE
[23]   X PLOT INT AND NEW VS T
[24]   W$SWIDTH 70
[25]   'NEW ';NEW
[26]   'INT ';INT
[27]   W$SWIDTH 132
[28]   $GGO
[29]  STOP:FIFREE 1
[30]   $GO
   $F
[31]   $F
```

```
$FCONVERT[¤]
   $F T$SCONVERT X
[1]    $G(12=$RX)/ZERO
[2]    T$S($E10ΔX)#10*$E10$ΔX
[3]    $GO
[4]   ZERO:T$S0
[5]    $GO
   $F
[6]   $F
```

```
LIST
1 DIM X(25),Y(25),Z(25),S(25)
5 PRINT "ENTER NO. OF DATA POINTS IN SET"\INPUT K
10 PRINT "ENTER TIME AND INTENSITY DATA"
15 FOR I=1 TO K\INPUT X(I),Z(I)
16 Y(I)=LOG(Z(I))/2.303\NEXT I
27 PRINT "ENTER MINIMUM NO. OF POINTS TO BE CONSIDERED"\INPUT N
28 N=N+1
29 A=0\B=0\C=0\D=0\E=0\F=0\G=0\H=0
34 FOR I=1 TO N
35 A=A+Y(I)\B=B+X(I)\E=E+X(I)*Y(I)\F=F+(A*B)/N\G=G+(X(I)↑2)
36 NEXT I
40 H=H+(Y(I)↑2)\C=C+B/N\D=D+A/N
45 P=E-(A*B)/N\Q=G-(B↑2)/N
50 M=P/Q\M1=D-M*C\T=-1/(2.303*M)
55 PRINT "SLOPE=",M,"INTERCEPT=",M1,"LIFETIME=",T,"MSEC"
56 PRINT " THE NO. OF POINTS USED =",N
60 FOR I=1 TO N\P=(M*X(I))+M1\S(I)=(P-Y(I))
75 NEXT I
80 S1=0\FOR I=1 TO N\S1=S1+S(I)\NEXT I\PRINT "SUM OF RESIDUALS",S1
81 IF N<K THEN 28 \GO TO 83
83 PRINT "ENTER 1 FOR BASELINE CORRECTION OR 2 TO STOP"\INPUT Z1
84 IF Z1=1 THEN 215 \IF Z1=2 THEN 85 \GO TO 1
85 STOP
215 PRINT "BASELINE CORRECTION PROGRAM"
220 DIM X(15),Y(15),Z(15),B(15),Q(15)
221 FOR I=1 TO 15\X(I)=0\Y(I)=0\Z(I)=0\B(I)=0\Q(I)=0\NEXT I
225 PRINT "ENTER SLOPE, INTERCEPT,& NO. OF POINTS TO BE CORRECTED"
226 INPUT M,M1,N\G=10↑M1
231 PRINT "ACTUAL INTERCEPT=",G
235 PRINT "ENTER TIME & INTENSITY TO BE CORRECTED"
240 FOR I=1 TO N\INPUT X(I),Y(I)\Z(I)=LOG(Y(I))/2.303
245 B(I)=10↑((M*X(I))+M1)\Q(I)=Y(I)-B(I)\NEXT I
250 PRINT "TIME","OLD INT","EXT BASELINE","NEW INT"
255 FOR I=1 TO N\PRINT X(I),Y(I),B(I),Q(I)
260 NEXT I\STOP
```

APPENDIX III

CALCULATION OF QUANTUM YIELD OF SOLID SO_2 AT 77°K AND 4.2°K

Quantum Yield Standard	Unknown	Quantum Yield of Standard	Intensity Ratio Unknown:Standard	Refractive Index Correction	Quantum Yield of Unknown
Anthracene in ethanol at 298°K	Anthracene in ethanol at 77°K	0.27 ± 0.03 [a]	561:302.5	None	0.50 ± 0.05
Anthracene in ethanol at 77°K	SO_2 at 77°K	0.50 ± 0.05	120:687.5	1.801/1.853 [a]	0.085 ± 0.004
Anthracene in ethanol at 4.2°K	SO_2 at 4.2°K	0.50 ± 0.05 [b]	508.3:221	1.801/1.853	0.625 ± 0.06
Benzophenone in EPA at 77°K	Benzophenone in cyclohexane at 77°K	0.74 ± 0.1 [c]	295:954.5	2.035/1.845	0.25 ± 0.03
Benzophenone in EPA at 77°K	SO_2 at 77°K	0.74 ± 0.1 [c]	120:954.5	1.801/1.845	0.088 ± 0.004
Benzophenone in cyclohexane at 4.2°K	SO_2 at 4.2°K	0.25 ± 0.03 [b]	221:510.5	1.801/2.035	0.575 ± 0.06

[a] See reference 31.

[b] Assumption made here that quantum yield of standard is the same at 4.2°K as it is at 77°K. In actuality it may be somewhat larger.

[c] See reference 32.

APPENDIX III

CALCULATION OF QUANTUM YIELD OF SOLID SO_2 AT 77°K AND 4.2°K

EXAMPLE: Quantum yield of SO_2 at 77°K relative to anthracene in ethanol at 77°K

$$\tau_p = (0.50 \pm 0.05)\left(\frac{120}{687.5}\right)\left(\frac{1.801}{1.853}\right) = 0.085 \pm 0.004$$

APPENDIX IV

PHOSPHORESCENCE LIFETIMES AT 77°K FOR SOLID $S^{16}O_2$ AND $S^{18}O_2$

$\tau_p(S^{16}O_2)$, msec	$\tau_p(S^{18}O_2)$
1.061	1.417
1.040	1.526
1.055	1.337
1.197	1.098
1.115	1.079
0.758	1.299
0.759	1.324
0.844	1.424
0.740	1.504
0.765	1.516
1.113	1.398
1.134	1.408
1.044	1.432
1.078	1.185
1.083	1.136
0.994	1.189
1.064	1.104
1.063	1.172
0.966	1.154
0.945	1.032
0.944	1.137
1.008	
Average = 0.9895 ± 0.1087	1.280 ± 0.1440
% Uncertainty = 11%	11%

Magnitude of Isotope Effect = 29%

APPENDIX V

PHOSPHORESCENCE LIFETIMES FOR SOLID $S^{16}O_2$ AND $S^{18}O_2$ AT 4.2°K

τ_p ($S^{16}O_2$), msec	τ_p ($S^{18}O_2$), msec
8.373	9.328
8.645	10.447
8.480	9.546
8.643	9.208
8.988	9.871
8.754	9.984
8.633	
8.601	
8.938	
8.706	
Average = 8.676 ± 0.136	9.731 ± 0.370
Percent Uncertainty = 1.6%	3.8%
Isotope Effect = 12%	

APPENDIX VI

CALCULATION OF RADIATIVE RATE CONSTANT (k_r) AND NONRADIATIVE RATE CONSTANT (k_{nr})

EXAMPLE: $S^{16}O_2$ at 77°K

Quantum yield of phosphorescence for solid SO_2 at 77°K (ϕ_p)

$= 0.088 \pm 0.004$

Phosphorescence lifetime (τ_p) for solid $S^{16}O_2$ at 77°K

$= 0.9895 \pm 0.1087$ msec

By definition,

$$\tau_p = (k_r + k_{nr})^{-1} \tag{11}$$

and

$$\phi_p = \frac{k_r}{k_r + k_{nr}} \tag{12}$$

Therefore,

$$k_R = \frac{\phi_p}{\tau_p} = \frac{0.088 \pm 0.004}{0.9895 \pm 0.1087 \text{ msec}} = 0.0889 \pm 0.0138 \text{ msec}^{-1}$$

$$0.089 \pm 0.014 \text{ msec}^{-1}$$

$$k_{nr} = \frac{1}{\tau_p} - k_r \tag{14}$$

$$= \frac{1}{0.9895 \pm 0.1087 \text{ msec}} - 0.0889 \pm 0.0138 \text{ msec}^{-1}$$

$$= 0.9217 \pm 0.1248 \text{ msec}^{-1}$$

$$0.922 \pm 0.125 \text{ msec}^{-1}$$

APPENDIX VII

PHOSPHORESCENCE LIFETIMES FOR SOLID $S^{16}O_2$ AND $S^{18}O_2$ AT 1.4°K

$S^{16}O_2$	τ_1, msec	τ_2, msec	τ_3, msec
	1.2	6.2	34.8
	1.3	7.7	34.5
	1.3	7.0	37.1
	1.2	6.4	37.0
AVERAGE =	35.9 ± 1.2	6.8 ± 0.5	1.3 ± 0.05
UNCERTAINTY AS A % =	3.8%	7.3%	3.3%

$S^{18}O_2$	τ_1, msec	τ_2, msec	τ_3, msec
	2.0	6.0	62.6
	1.6	5.6	68.5
	1.4	5.7	53.7
	1.2	5.0	47.7
	2.2	5.9	64.3
AVERAGE =	59.4 ± 6.9	5.6 ± 0.3	1.7 ± 0.3
UNCERTAINTY AS A %	17%	5.4%	11.6%

BIBLIOGRAPHY

1. C. A. Hutchison and B. W. Mangum, J. Chem. Phys. 32, 1261 (1960).
2. G. W. Robinson, J. Mol. Spectrosc. 6, 58 (1961).
3. J. C. Miller and R. F. Borkman, J. Chem. Phys. 56, 3727 (1972).
4. T. E. Martin and A. H. Kalantar, J. Chem. Phys. 48, 4996 (1968).
5. R. F. Borkman and D. R. Kearns, J. Chem. Phys. 44, 945 (1966).
6. A. A. Lamola, J. Chem. Phys. 47, 4810 (1967).
7. N. J. Turro and R. Engel, J. Am. Chem. Soc. 90, 2989 (1968).
8. R. F. Borkman, Chem. Phys. Letters 9, 77 (1971).
9. N. C. Yang, S. L. Murov, and T. C. Shieh, Chem. Phys. Letters 3, 6 (1969).
10. J. Simpson and H. Offen, Mol. Photochem. 2, 115 (1970).
11. T. E. Martin and A. H. Kalantar, Chem. Phys. Letters 1, 623 (1968); 4, 235 (1969).
12. J. W. Rabalais, H. J. Maria, and S. P. McGlynn, Chem. Phys. Letters 3, 59 (1969); J. Chem. Phys. 51, 2259 (1969).
13. J. D. Laposa and H. Singh, Chem. Phys. Letters 4, 288 (1969).
14. S. H. Lin and R. Bersohn, J. Chem. Phys. 48, 2732 (1968).
15. J. D. Simpson, H. W. Offen, and J. G. Burr, Chem. Phys. Letters 2, 383 (1968).
16. B. S. Yamanashi and R. F. Borkman, Chem. Phys. Letters 13, 592 (1972).
17. G. Herzberg, Electronic Spectra of Polyatomic Molecules, (D. van Nostrand, Princeton, 1966), pp. 500-504, 507-513.
18. N. Metropolis and H. Beutler, Phys. Rev. 57, 1078 (1940).
19. A. J. Merer, Disc. Far. Soc. 35, 127 and 226-230 (1963).
20. J. C. D. Brand, V. T. Jones, and C. diLauro, J. Mol. Spectrosc. 40, 616 (1971).

21. K. Srikameswaran and J. C. D. Brand, 27th Symposium on Molecular Structure and Spectroscopy, Columbus, Ohio, 1972.

22. J. L. Hardwick, "The Magnetic Rotation Spectrum of Sulfur Dioxide in the 3000 Å region," Ph.D. Dissertation, Georgia Institute of Technology, 1972.

23. R. M. Hochstrasser and A. P. Marchetti, J. Mol. Spectrosc. 35, 335 (1970).

24. L. F. Phillips, J. J. Smith, and B. Meyer, J. Mol. Spectrosc. 29, 230 (1969).

25. H. D. Mettee, J. Chem. Phys. 49, 1784 (1968).

26. T. N. Rao, S. S. Collier, and J. G. Calvert, J. Am. Chem. Soc. 91, 7 (1969).

27. W. H. Eberhardt, J. Opt. Soc. Amer. 40, 172 (1950).

28. U.S. Dept. of Commerce Monograph #10, "1958 Helium Scale of Temperatures," H. vanDijk, N. Durieux, J. R. Clement, and J. K. Logan.

29. C. A. Parker, Photoluminescence of Solutions, (Elsevier, New York, 1968), p. 263.

30. G. Friedlander, J. W. Kennedy, and J. M. Miller, Nuclear and Radiochemistry, (Wiley, New York, 1964), pp. 69-71.

31. J. N. Demas and G. A. Crosby, J. Phys. Chem. 75, 991 (1971).

32. E. H. Gilmore, G. E. Gibson, and D. S. McClure, J. Chem. Phys. 20, 829 (1952); 23, 399 (1955).

33. D. S. Tinti, Chem. Phys. Letters 12, 169 (1971).

34. S. J. Strickler and D. B. Howell, J. Chem. Phys. 49, 1947 (1968).

35. B. Meyer, L. F. Phillips, and J. J. Smith, Proc. N.A.S. 61, 7 (1968).

36. K. F. Greenough and A. B. F. Duncan, J. Am. Chem. Soc. 83, 555 (1961).

37. J. C. D. Brand and R. Nanes, J. Mol. Spectrosc. 46, 194 (1973).

38. G. Herzberg, Infrared and Raman Spectra of Polyatomic Molecules, (van Nostrand Reinhold, New York, 1945), pp. 168-172.

39. A. J. Merer, Disc. Far. Soc. 35, 127 (1963).

40. R. P. Bauman, Absorption Spectroscopy, (Wiley, New York, 1962), p. 541.

41. S. J. Strickler and R. A. Berg, J. Chem. Phys. 37, 814 (1962).

42. W. Kauzmann, Quantum Chemistry, (Academic Press, New York, 1967), p. 581.

43. Unpublished results of R. M. Hochstrasser and A. P. Marchetti.

44. B. Meyer, Low Temperature Spectroscopy, (Elsevier, New York, 1971), pp. 66-7, 101.

45. M. A. El-Sayed, et al., J. Chem. Phys. 48, 1395 (1968).

46. D. F. Heller, K. F. Freed, and W. M. Gelbhart, J. Chem. Phys. 56, 2309 (1971).

47. R. S. Mulliken (private communication with J. B. Coon), Can. J. Chem. 36, 10 (1958).

48. P. M. Johnson and L. Zeigler, J. Chem. Phys. 56, 2169 (1972).

49. S. F. Fischer and E. C. Lim, Chem. Phys. Letters 14, 40 (1972).

50. H. Kayser, Tabelle der Schmingungszahlen, (Edwards Brothers, Ann Arbor, Michigan, 1944).

51. A. B. Zahlan, editor, The Triplet State, (Cambridge University Press, 1967), p. 427.

52. R. K. Russell, B. L. Landrum, and E. E. Vezey, A Vibrational Analysis of the 3800 Å Absorption System of Sulphur Dioxide, (Air Force Technical Note, Air Research & Development Command, 1956).

53. W. C. Gardner, Rates and Mechanisms of Chemical Reactions, (Benjamin, New York, 1969), p. 70.